

Conformalized Bayesian Inference, with Applications to Random Partition Models

Nicola Barilett* Nhat Ho Alessandro Rinaldo

Department of Statistics and Data Sciences, UT Austin

December 22, 2025

Abstract

Bayesian posterior distributions naturally represent parameter uncertainty informed by data. However, when the parameter space is complex, as in many nonparametric settings where it is infinite-dimensional or combinatorially large, standard summaries such as posterior means, credible intervals, or simple notions of multimodality are often unavailable, hindering interpretable posterior uncertainty quantification. We introduce Conformalized Bayesian Inference (CBI), a broadly applicable and computationally efficient framework for posterior inference on nonstandard parameter spaces. CBI yields a point estimate, a credible region with assumption-free posterior coverage guarantees, and a principled analysis of posterior multimodality, requiring only Monte Carlo samples from the posterior and a notion of discrepancy between parameters. The method builds a pseudo-density score for each parameter value, yielding a MAP-like point estimate and a credible region derived from conformal prediction principles. The key conceptual step underlying this construction is the reinterpretation of posterior inference as prediction on the parameter space. A final density-based clustering step identifies representative posterior modes. We investigate a number of theoretical and methodological properties of CBI and demonstrate its practicality, scalability, and versatility in simulated and real data clustering applications with random partition models. An accompanying Python library, `cbi_partitions`, is available at https://github.com/nbarilett/cbi_partitions_repo.¹

Keywords: Bayesian Clustering, Bayesian Nonparametrics, Conformal Prediction, Monte Carlo Methods, Multimodality.

*The authors are grateful to Mario Beraha, Michele Guindani, Peter Müller, Khai Nguyen, Pratik Patil and Stephen G. Walker for their insightful comments, and to Yunshan Duan, Ziyi Song and Wenyi Wang for sharing their model outputs used for the real data applications presented in the paper.

¹A step-by-step tutorial is found at https://nbarilett.github.io/cbi_partitions_repo/.

1 Introduction

Bayesian statistical methods have become a standard tool in probabilistic modeling, primarily due to their natural ability to represent uncertainty in the phenomena under study. In the Bayesian framework, the generative process underlying the observed data is formalized as a statistical model with parameters to be inferred from the data. Uncertainty about these parameters is expressed through a prior distribution, which is updated to the posterior distribution given the data, and subsequently to the predictive distribution for unseen observations. A central advantage of the Bayesian framework is that, when inference is required over a parameter space Θ indexing the statistical model, it is enough to specify a prior probability distribution on Θ and to compute, often approximately (for instance, via Monte Carlo methods), the corresponding posterior distribution. This provides a coherent basis for point estimation—selecting a single parameter value that summarizes the posterior distribution—and uncertainty quantification—characterizing the regions of Θ on which the posterior places significant mass. This paradigm has proven particularly powerful in the nonparametric setting, where modeling flexibility is achieved by allowing Θ to be a complex, and often infinite-dimensional, parameter space.

This abstract flexibility, however, often comes at the price of some practical difficulties. While parameter spaces associated with flexible priors can capture complex aspects of the data-generating process, they may lack a conventional structure (for example, a vector or ordering structure) that allows for an interpretable summary of the posterior distribution through quantities such as a posterior mean/mode or a credible interval/band. This challenge is pervasive. Consider, for instance, models whose parameter spaces consist of data partitions (Wade 2023), covariance matrices (Leonard & Hsu 1992, Yang & Berger 1994), graphs (Nowicki & Snijders 2001, Orbanz & Roy 2014), mixing measures (Nguyen 2013), among innumerable other examples. In such cases, although Monte Carlo methods, often in

the form of Markov Chain Monte Carlo (shortened to MCMC, [Metropolis et al. 1953](#), [Hastings 1970](#), [Tierney 1994](#), [Gamerman & Lopes 2006](#)), provide good empirical approximations of the posterior distribution, the complexity of the sampled objects hinders interpretable inference. This raises a few fundamental questions: What constitutes a suitable point estimate of the random parameter $\theta \in \Theta$ under the posterior distribution? How can one define a credible region with reasonable size and a prescribed posterior coverage level? Is the posterior distribution concentrated in a single, homogeneous region of Θ , or does it assign substantial mass to multiple distinct regions? When only Monte Carlo samples are available and the parameter space lacks a familiar Euclidean-like structure, no general or obvious answers exist to these questions.

For specific instances of complex parameter spaces, these challenges have motivated a variety of solutions, ranging from theoretically grounded to ad hoc. For example, in point estimation, a common decision-theoretic approach specifies a loss function on $\Theta \times \Theta$ and selects the minimizer of the posterior expected loss, typically approximated through Monte Carlo sampling ([Bernardo & Smith 1994](#)). In contrast, questions concerning credible regions and posterior multimodality are often addressed through problem-specific heuristics that exploit the structure of Θ . For instance, when Θ denotes the space of data clusterings arising from random partition models, several tailored approaches have been proposed ([Wade & Ghahramani 2018](#), [Balocchi & Wade 2025](#)); since random partition models will serve as our main illustrative application, we defer a detailed discussion of these methods. A useful strategy is to examine low-dimensional aspects of the parameter ([Woody et al. 2021](#), [Bolafine et al. 2025](#)), but while this can offer preliminary insight into posterior uncertainty, it risks discarding the very flexibility afforded by using a rich parameter space Θ . It is therefore desirable to develop general and principled frameworks for addressing these questions simultaneously, coherently, and efficiently, given only Monte Carlo samples from a

posterior distribution over Θ .

In this article, we make a step in this direction by introducing a broadly applicable methodology grounded in the theories of conformal prediction (Vovk et al. 2005, Shafer & Vovk 2008, Angelopoulos & Bates 2023) and density-based clustering (Rodriguez & Laio 2014, Ester et al. 1996, Kriegel et al. 2011), which we term *Conformalized Bayesian Inference (CBI)*. The proposed pipeline is as follows. Assume that, given a posterior distribution Π on Θ , we have at our disposal $T \in \mathbb{N}$ independent and identically distributed (iid) Monte Carlo samples $\theta = \{\theta_1, \dots, \theta_T\}$, each marginally distributed according to Π . The iid assumption may be either true exactly by the nature of the adopted Monte Carlo scheme, or can be thought to hold approximately in the case of MCMC samples, as long as the sampler chain has been properly thinned (see Theorem 2 below). We then split the samples into two subsets: a training set $\theta^1 = \{\theta_1, \dots, \theta_S\}$ and a calibration set $\theta^2 = \{\theta_{S+1}, \dots, \theta_T\}$. The key idea is to compute, for each calibration sample $\theta \in \theta^2$, a pseudo-density score

$$\theta \mapsto s(\theta; \theta^1) \in \mathbb{R},$$

which is estimated using the training set θ^1 and is designed to capture a notion of likelihood or density of θ under the posterior distribution. This will be achieved by defining $s(\cdot; \theta^1)$ as a kernel density estimator (KDE) based on a discrepancy $\mathcal{D} : \Theta \times \Theta \rightarrow \mathbb{R}_+$ between parameters.

Once the scoring rule is available, the CBI framework proceeds through the following three main steps:

- *Step 1: point estimation.* The calibration scores can be used to define an intuitive point estimator. Specifically, we select

$$\theta_* \in \arg \max_{\theta \in \theta^2} s(\theta; \theta^1).$$

Because $s(\cdot; \theta^1)$ is a posterior pseudo-density function, θ_\star may be interpreted as a pseudo-maximum-a-posteriori (pseudo-MAP) estimator.

- *Step 2: credible region.* By exchangeability of the calibration scores, standard conformal prediction arguments yield a credible region $\mathcal{C}_{1-\alpha}(\theta^2) \subseteq \Theta$, based on the quantiles of $\{s(\theta; \theta^1) : \theta \in \theta^2\}$, having a prescribed $(1 - \alpha) \times 100\%$ coverage under Π (for $\alpha \in (0, 1)$, in a precise statistical sense to be defined later). The key conceptual step leading to this construction is the reinterpretation of inference based on posterior Monte Carlo samples as prediction on the parameter space according to the posterior distribution, and to leverage conformal prediction tools accordingly. Two appealing features of this procedure are that (i) the attached coverage guarantee is independent of any feature of the target posterior Π , accommodating parameter spaces of arbitrary dimension and with almost no structure, and (ii) for a new sample θ , it provides a simple way to define a standardized measure of *typicality* $\hat{p}(\theta; \theta^2) \in [0, 1]$ under Π , which may also be formally interpreted as a p -value under an intuitive distributional null hypothesis.
- *Step 3: multimodality analysis.* Finally, the interpretation of $\theta \mapsto s(\theta; \theta^1)$ as a posterior pseudo-density function allows one to explore the possibly multimodal structure of the posterior distribution through density-based clustering techniques. By equipping Θ with the discrepancy \mathcal{D} , one can identify distinct high-density regions, thereby revealing whether the posterior distribution places substantial mass around multiple, well-separated parameter values.

Throughout the paper, we will focus on developing simple, robust, and efficient methods to compute the calibration scores and to carry out the multimodality analysis. As will become evident, the advantages of our methodology include a high degree of intuitiveness and flexibility (for example, in the choice of the metric \mathcal{D} , or in the ability to restrict point

estimation to regions of Θ that the user considers plausible or of interest), as well as the potential for efficient implementation thanks to the parallelizability of score and distance computations.

While CBI can be described in full generality without reference to any particular statistical model, it is useful to ground the discussion in a concrete setting involving a parameter space Θ of interest. Therefore, before presenting a general treatment of CBI, in Section 2 we first introduce a fundamental class of models, namely random partition models, on which the strengths of our methodology can be clearly demonstrated. One advantage of working with random partition models is the existence of a rich literature addressing point estimation and uncertainty quantification based on posterior Monte Carlo samples over the space of data partitions (Wade & Ghahramani 2018, Wade 2023, Balocchi & Wade 2025), providing a natural conceptual benchmark for our discussion. Moreover, since clustering is an inherently difficult problem (Hennig 2015), Bayesian posteriors over data partitions often display substantial uncertainty, frequently in the form of multimodality, which our framework is specifically designed to handle. After this, in Sections 3, 4, and 5 we describe CBI in detail and illustrate it with simulated data analyzed with random partition models.² Section 6 showcases two real-world applications of CBI to Bayesian clustering of (i) the classical Galaxy velocities dataset (Roeder 1990), and (ii) event-related potential (ERP) waveform functional data (Song et al. 2025, Kappenman et al. 2021). Section 7 concludes the article with a discussion of the current limitations and future directions related to CBI.

²However, see the Supplementary Material for two additional experiments applying CBI to models where the parameter space consists of discrete mixing measures endowed with the Wasserstein-1 distance (Nguyen 2013, Villani et al. 2008) and covariance matrices endowed with the operator norm distance.

2 Motivation: random partition models

Given a data set X_1, \dots, X_n , a fundamental unsupervised statistical learning problem consists in partitioning the data into disjoint clusters representing heterogeneous subpopulations. Denoting by Θ the space of partitions of the data, the Bayesian framework tackles the clustering problem by specifying a prior $\pi(\theta)$ over Θ and a likelihood $p(X_1, \dots, X_n | \theta)$ for the observations given their partitioning according to $\theta \in \Theta$. The resulting posterior distribution

$$\Pi(\theta) \propto p(X_1, \dots, X_n | \theta) \pi(\theta)$$

allows for coherent inference on the clustering structure of the observed data. In practice, inference on clustering may be formulated at the latent level of a hierarchical density mixture model, where heterogeneity among subpopulations is interpreted as observations being generated from different components of a mixture model (Fruhwirth-Schnatter et al. 2019, Lo 1984, Escobar & West 1995, Lijoi et al. 2005, Barrios et al. 2013, Lijoi et al. 2020), or, more recently, through approaches based on tailored losses (Rigon et al. 2023) or level sets (Buch et al. 2024). We refer the reader to Wade (2023), Grazian (2023), and the review section of Balocchi & Wade (2025) for comprehensive and up-to-date overviews of the field.

The combinatorially large size of Θ typically prevents exact posterior evaluation, and approximate computational methods, most often in the form of MCMC sampling, are adopted instead. For instance, if the random partition model is specified within a hierarchical mixture framework, standard samplers (Escobar & West 1995, 1998, MacEachern & Müller 1998, Favaro & Teh 2013, Neal 2000) will, at each iteration $t = 1, \dots, T$, draw a sample $\theta_t \sim \Pi$ (in addition to sampling the other mixture parameters). These samples are usually stored as vectors of cluster assignments $C_t = (c_{t1}, \dots, c_{tn})$, encoding the partition (equivalence) relation \sim_{θ_t} via $X_i \sim_{\theta_t} X_j$ if and only if $c_{ti} = c_{tj}$, for all $i, j = 1, \dots, n$. Assuming appropriate thinning of the chain and a warm start $\theta_1 \sim \Pi$, the resulting samples $\theta_1, \dots, \theta_T$

will serve as the basis of our CBI procedure.

A widely used metric on the space of partitions Θ is the Variation-of-Information (VI) metric (Meilă 2007), denoted by \mathcal{D}_{VI} and defined as follows. Take any two partitions $\theta, \theta' \in \Theta$ with associated cluster assignment vectors C, C' and respective numbers of clusters K and K' . Let $\{\bar{c}_1, \dots, \bar{c}_K\}$ and $\{\bar{c}'_1, \dots, \bar{c}'_{K'}\}$ denote the sets of unique cluster labels in each vector, and define $n_{j,*} := |\{i = 1, \dots, n : c_i = \bar{c}_j\}|$, $n_{*,k} := |\{i = 1, \dots, n : c'_i = \bar{c}'_k\}|$, and $n_{j,k} := |\{i = 1, \dots, n : c_i = \bar{c}_j, c'_i = \bar{c}'_k\}|$, for all $j = 1, \dots, K$ and $k = 1, \dots, K'$. Then,

$$\mathcal{D}_{VI}(\theta, \theta') := \quad (1)$$

$$- \sum_{j=1}^K \frac{n_{j,*}}{n} \log_2 \left(\frac{n_{j,*}}{n} \right) - \sum_{k=1}^{K'} \frac{n_{*,k}}{n} \log_2 \left(\frac{n_{*,k}}{n} \right) - 2 \sum_{j=1}^K \sum_{k=1}^{K'} \frac{n_{j,k}}{n} \log_2 \left(\frac{n \cdot n_{j,k}}{n_{j,*} \cdot n_{*,k}} \right).$$

Meilă (2007) showed that \mathcal{D}_{VI} is a proper metric on Θ , and that it enjoys several appealing theoretical properties, such as its information-theoretic interpretation in terms of self-entropy and cross-entropy between partitions, while also being efficiently computable. Although alternative discrepancy measures have been proposed, such as the Binder loss (Binder 1978, Dahl 2006, Lau & Green 2007), the adjusted Rand index (Fritsch & Ickstadt 2009), the normalized VI (Vinh et al. 2010, Rastelli & Friel 2018), and more (Quintana & Iglesias 2003, Dahl et al. 2022, Nguyen & Mueller 2024), we focus on the VI metric in what follows, given its widespread use and well-established role as the standard metric in Bayesian clustering.

The large size of Θ and its discrete nature make it an ideal example of a setting where point estimation and posterior uncertainty quantification are highly non-trivial, even when Monte Carlo samples from Π are available. The popularity of clustering and the success of Bayesian approaches in this domain have given rise to an extensive literature on the topic. A seminal contribution is due to Wade & Ghahramani (2018), who popularized the use of the VI metric in Bayesian clustering and proposed to address point estimation via posterior

expected VI minimization, while constructing (approximations of) VI credible balls with prescribed posterior mass for uncertainty quantification.³ Computational and theoretical extensions of this framework, often but not exclusively focused on point estimation, include [Rastelli & Friel \(2018\)](#), [Dahl et al. \(2022\)](#), [Nguyen & Mueller \(2024\)](#), [Buch et al. \(2024\)](#), among others. An insightful perspective was recently introduced by [Balocchi & Wade \(2025\)](#), who emphasized the importance of accounting for multimodality in the posterior distribution over Θ and proposed summarizing Π with the closest L -atom mixture of point masses in the Wasserstein-over-VI metric, yielding a fixed number L of representative partitions corresponding to the distinct posterior modes.

As this discussion highlights, Bayesian random partition models, where inference takes place over the complex space of data clusterings, provide an ideal application for a methodology such as ours, which aims to facilitate inference from posterior Monte Carlo samples precisely in settings where point estimation and uncertainty quantification are far from straightforward. We are now ready to describe our methodology.

3 Conformalized Bayesian Inference: preliminaries and point estimation

Recall the problem we aim to solve: given iid posterior Monte Carlo samples θ , split into a training subset θ^1 and a calibration subset θ^2 , how can we perform point estimation and uncertainty quantification in practice? Following the pipeline described in the introduction, the first key step is to define a scoring function $\theta \mapsto s(\theta; \theta^1)$ that captures a notion of pseudo-density ([Ferraty & Vieu 2006](#)) under the posterior distribution. We now propose a simple and robust solution.

³See also the contemporaneous and independent preprint by [Page et al. \(2025\)](#).

We begin by choosing a metric \mathcal{D} on Θ .⁴ In many nonparametric inference problems, although the parameter space may have a nonstandard structure, it is often possible to define a meaningful distance between any two elements. This is the case for the VI metric between partitions, but similar constructions exist for covariance matrices (operator norm distance), graphs (graph edit distance, spectral distances, etc.), mixing measures (Wasserstein distances), and densities (\mathcal{L}^p distances), among others. Given such a choice of \mathcal{D} , we define the following scoring rule.

Definition 1. *Let $\theta, \theta' \in \Theta$. The \mathcal{D} -KDE score $s(\theta; \theta^1)$ with hyperparameter $\gamma > 0$ is given by*

$$s(\theta; \theta^1) := \frac{1}{S} \sum_{t=1}^S \mathcal{K}(\theta, \theta_t), \quad \mathcal{K}(\theta, \theta') := e^{-\gamma \mathcal{D}(\theta, \theta')}.$$

Intuitively, $s(\cdot; \theta^1)$ acts as a KDE score, but with the Euclidean norm replaced by the metric \mathcal{D} to handle the possibly complex parameters in Θ (Schölkopf & Smola 2001, Shawe-Taylor & Cristianini 2004). Under certain conditions on (Θ, \mathcal{D}) , one can have $\mathcal{D}(\theta, \theta') = \|\phi(\theta) - \phi(\theta')\|$ for some isometric embedding $\phi : \Theta \rightarrow \mathbb{R}^E$ and $E \in \mathbb{N}$, at least for certain θ, θ' (Schoenberg 1935). Thus, the proposed score can be viewed—formally in some cases, loosely in general—as a two-step procedure: first embedding parameters into a latent Euclidean space that preserves the geometry induced by \mathcal{D} , and then performing KDE in that space.

While other scoring rules can be devised, \mathcal{D} -KDE provides a simple and robust baseline.⁵ It relies on a clearly defined metric that encodes a meaningful notion of distance between parameters (a computationally and/or conceptually valuable feature, depending on the context) and reduces the challenge of defining a pseudo-density score on a complex space Θ to a straightforward, efficiently implementable KDE computation. In particular, evaluating $\mathcal{K}(\theta, \theta_t)$ is easily parallelized across samples in the calibration and training sets. Optionally, computation can be further sped up by building the score, for each calibration sample, using

⁴This need not be a metric; any notion of discrepancy suffices in practice.

⁵A kernel different from $D \mapsto e^{-\gamma D}$ may also be chosen.

only a random subset of the training samples.

As mentioned in the introduction, after computing the calibration scores via the \mathcal{D} -KDE procedure, our proposed point estimate is

$$\theta_* \in \arg \max_{\theta \in \theta^2} s(\theta; \theta^1).$$

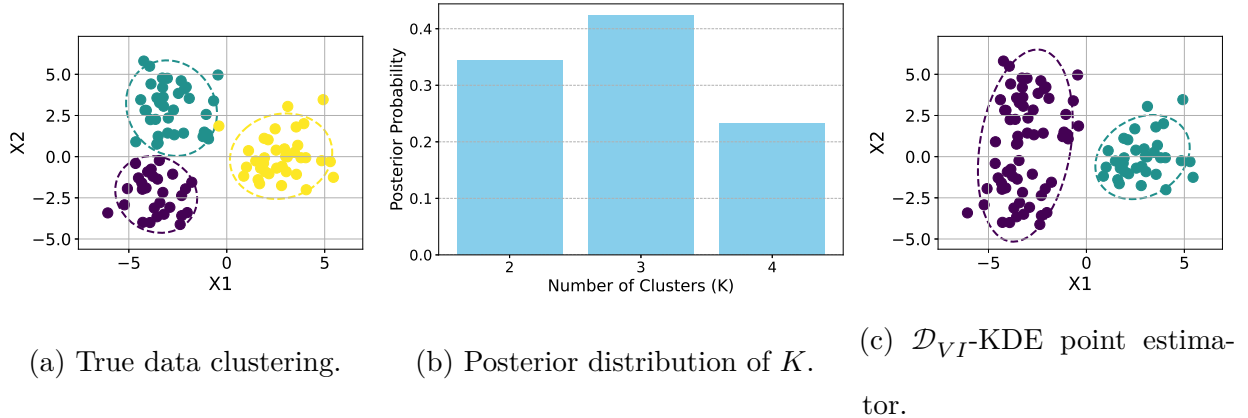
Because $s(\cdot; \theta^1)$ is constructed to act as a posterior KDE evaluation, θ_* can be interpreted as a kind of maximum-a-posteriori (MAP) estimator based on this posterior KDE. Of course, this interpretation should be taken with caution, since the posterior may not possess a proper or tractable density (as in random partition models, where the posterior over Θ is a probability mass function and the true MAP corresponds to the partition with the largest mass), although it provides a simple and efficient strategy to summarize the posterior with a single parameter value.

Another useful perspective is to view θ_* as a posterior expected loss minimizer restricted to the calibration set, with the only difference that the loss \mathcal{D} is transformed via $D \mapsto \exp\{-\gamma D\}$ to produce a pseudo-density score. In contexts such as random partition models, where efficient algorithms exist for exhaustive searches over Θ (Wade & Ghahramani 2018, Dahl et al. 2022), ideas from that literature can be used to extend the search for the score maximizer beyond the calibration set. Nonetheless, we believe that restricting the maximization to the calibration set remains appealing for several reasons: (i) the scores must in any case be computed (and can be parallelized) for the uncertainty quantification step based on conformal prediction (described later), making this approach more convenient than (possibly sequential) exhaustive search algorithms, especially when the primary goal is uncertainty quantification and point estimation serves only as a simple preliminary summary of the posterior; (ii) the calibration samples are drawn from the posterior and are therefore likely to achieve high scores in the first place, making exhaustive search potentially redundant; and (iii) the search can be flexibly customized—for example, in the

context of clustering, one may prefer focusing on partitions with at most three scientifically interpretable clusters, in which case the score maximization can be restricted to the subset of calibration samples satisfying the desired properties. This allows the procedure to combine data-driven evidence with user-specified structural assumptions in a flexible and interpretable way.

Example 1. We draw 100 samples from a two-dimensional isotropic Gaussian mixture model with three equally weighted components, each with identity covariance matrix scaled by 1.5 and with respective mean vectors $(-3, -3)$, $(-3, 3)$, and $(3, 0)$. The simulation proceeds by first sampling component assignments and then generating the data according to the corresponding Gaussian component. Figure 1a visualizes the resulting “true” partition of the data based on these component assignments.

Figure 1: Gaussian mixture simulated data, analyzed using a PY Gaussian density mixture model.



The data are then analyzed by fitting a Gaussian mixture model with a Pitman-Yor process prior on the mixing measure (Pitman & Yor 1997, Perman et al. 1992, De Blasi et al. 2013), using a concentration parameter of 0.03 and a discount parameter of 0.01. A standard marginal Gibbs sampler is applied via the Python package `pyrichlet` (Selva et al. 2025), and after burn-in and thinning, 5,000 training partitions and 1,000 calibration partitions

are retained.

Figure 1b shows the posterior distribution of K , the number of distinct clusters to which the 100 data points are assigned. The histogram suggests that the values 2, 3, and 4 all receive substantial posterior mass, indicating the presence of potential uncertainty in the clustering. Figure 1c displays the partition corresponding to the \mathcal{D}_{VI} -KDE point estimate (with hyperparameter $\gamma = 0.5$). This estimate essentially coincides with the true clustering once the two left-most clusters are collapsed together.⁶ Notably, this occurs even though partitions with 3 clusters receive more posterior mass than those with 2 clusters (see Figure 1b). This behavior may be due to many sampled partitions with 3 clusters being very close to the point estimator (e.g., differing from it by only a few cluster assignments), or because the VI metric inherently favors parsimonious clusterings by weighting larger clusters more heavily; see Equation (1). A clearer picture will emerge with our upcoming discussion of posterior uncertainty quantification beyond point estimation.

4 Credible region

While point estimation provides a useful first summary of the posterior distribution, it necessarily omits the uncertainty encoded in the full posterior. To address this, a key component of our CBI methodology is the construction of a credible posterior subset of Θ based on the principles of conformal prediction (Vovk et al. 2005, Shafer & Vovk 2008, Lei et al. 2018, Angelopoulos & Bates 2023). Very briefly, conformal prediction in its basic form allows one to construct a set-valued prediction for the next observation given the first N samples from an exchangeable sequence, with a precisely defined, finite-sample, and distribution-free coverage guarantee. In our context, the crucial step is to interpret

⁶In the rest of the paper, we will refer to the partitions pictured in Figures 1a and 1c as the “true partition” and the “collapsed partition,” respectively.

Monte Carlo samples as draws from an exchangeable sequence, and to recast the problem of constructing a posterior credible region as that of predicting a region where a new independent posterior sample would fall with high probability.⁷ We now formalize this intuition.

Recall our assumption that the available samples from Π , and in particular the calibration samples $\theta^2 = (\theta_{S+1}, \dots, \theta_T)$ (for convenience, let $N := T - S$), are iid. See Proposition 2 for a theoretical justification of this assumption when the original sampler features Markov dependence, as in MCMC. Define

$$\hat{p}(\theta; \theta^2) := \frac{|\{\theta' \in \theta^2 : s(\theta; \theta^1) \geq s(\theta'; \theta^1)\}| + 1}{N + 1}. \quad (2)$$

Then, for any error rate $\alpha \in (0, 1)$, the corresponding credible region is

$$\mathcal{C}_{1-\alpha}(\theta^2) := \{\theta \in \Theta : \hat{p}(\theta; \theta^1) \geq \alpha\}. \quad (3)$$

In words, we declare $\theta \in \Theta$ to belong to the credible region $\mathcal{C}_{1-\alpha}(\theta^2)$ if its \mathcal{D} -KDE score is not too low compared to those of the calibration samples—that is, if it is not too “unlikely” under the posterior relative to samples known to be drawn from it. Note that we emphasize the dependence of the credible region on the calibration set but not on the training set. This is because, from now on, the latter is treated as fixed (or, equivalently, we condition on its realization), since the coverage guarantees to be discussed do not depend on any particular scoring rule. The following proposition states precisely the coverage property ensured by $\mathcal{C}_{1-\alpha}(\theta^2)$.

Proposition 1. *The set $\mathcal{C}_{1-\alpha}(\theta^2)$ satisfies*

$$\mathbb{P}_{(\theta^2, \theta) \stackrel{\text{iid}}{\sim} \Pi} [\theta \in \mathcal{C}_{1-\alpha}(\theta^2)] \equiv \mathbb{E}_{\theta^2 \stackrel{\text{iid}}{\sim} \Pi} [\Pi(\mathcal{C}_{1-\alpha}(\theta^2))] \geq 1 - \alpha. \quad (4)$$

⁷We note that, although with entirely different goals (namely, calibrating predictions derived from Bayesian predictive distributions), conformal prediction has already been applied in the Bayesian setting, e.g., by [Fong & Holmes \(2021\)](#).

Furthermore, for any $\delta \in (0, 1)$, its posterior mass satisfies

$$|\Pi(\mathcal{C}_{1-\alpha}(\theta^2)) - (1 - \alpha)| \leq \frac{\max(\alpha, 1 - \alpha)}{N} + \left| \frac{k_{\alpha, N}}{N} - \hat{\Pi}_{s, N}(s_{(k_{\alpha, N})}^-) \right| + \sqrt{\frac{1}{2N} \ln \left(\frac{2}{\delta} \right)} \quad (5)$$

with $\mathbb{P}_{\theta^2 \stackrel{\text{iid}}{\sim} \Pi}$ -probability at least $1 - \delta$, where $k_{\alpha, N} := \lceil \alpha(N + 1) - 1 \rceil$, $s_{(k)}$ is the k -th order statistic of the calibration scores, and $\hat{\Pi}_{s, N}$ is their empirical cdf. Finally, $\hat{p}(\theta; \theta^2)$ satisfies

$$\forall \lambda \in [0, 1], \quad \mathbb{P}_{(\theta^2, \theta) \stackrel{\text{iid}}{\sim} \Pi} [\hat{p}(\theta; \theta^2) \leq \lambda] \leq \lambda. \quad (6)$$

Proposition 1 clarifies the rationale behind defining $\mathcal{C}_{1-\alpha}(\theta^2)$ as a credible region under the posterior Π with coverage $(1 - \alpha) \times 100\%$. In particular, Equation (4) ensures that the *entire procedure*, i.e., scoring the calibration samples and checking whether an independent draw from Π falls within $\mathcal{C}_{1-\alpha}(\theta^2)$, succeeds with probability at least $1 - \alpha$. Unsurprisingly, given its connection to conformal prediction, this construction has a frequentist flavor: it yields a distribution-free, finite-sample coverage guarantee under Π based on samples from it. From a purely subjective Bayesian standpoint, however, this raises no philosophical tension, since the task is to infer properties of the posterior distribution itself, which exists and is fixed, independently of whether the Bayesian model giving rise to it is meant to learn any true, fixed data-generating process. On the other hand, a key advantage of the conformal prediction approach is that the resulting coverage guarantee is not tied to any property of the posterior distribution. In particular, it does not rely on any specific topological or algebraic structure of Θ , which in many cases of interest may be non-standard, and remains valid regardless of the dimensionality of the posterior support, which in many of our motivating applications is extremely large or even infinite.

As Equation (4) shows, the coverage guarantee can also be interpreted as an expected-mass statement: the posterior mass of $\mathcal{C}_{1-\alpha}(\theta^2)$ exceeds $1 - \alpha$ *in expectation*, where the randomness arises from the calibration set. Thus, $\mathcal{C}_{1-\alpha}(\theta^2)$ is a random subset of Θ whose expected posterior mass is at least $1 - \alpha$. Equation (5) further characterizes the behavior of

this random set, showing that, with high probability, its posterior mass concentrates around $1 - \alpha$ at rate $N^{-1/2}$ in the calibration size N . Note that, unless the posterior distribution of the scores is atomless, the second term on the right-hand side of Equation (5) need not vanish as $N \rightarrow \infty$ (while it equals $1/N$ when the score distribution is continuous). This reflects the well-known fact that conformal quantile-based sets achieve coverage at least as high as the nominal level $1 - \alpha$, but may not approximate it tightly from above if atoms at specific quantiles exist in the target score distribution.

This notion of coverage differs from the traditional Bayesian definition, which concerns a fixed, non-random credible region \mathcal{C} satisfying $\Pi(\mathcal{C}) \geq 1 - \alpha$. Such a region, if computable and sufficiently small, would of course be preferable, as it would provide deterministic coverage. However, the very complexity of Θ that motivates our framework typically precludes analytical construction of such sets. Moreover, even conventional credible regions derived from Monte Carlo samples are inherently random, although this is rarely acknowledged explicitly: for instance, even a simple credible interval for a one-dimensional parameter (e.g., based on empirical upper- and lower-quantiles of Monte Carlo samples from the posterior distribution of that parameter) inherits randomness from the finite Monte Carlo sample size. From this point of view, a key advantage of our conformal construction is that it delivers rigorously defined, finite-sample posterior coverage guarantees, both in expectation (Equation (4)) and with high probability (Equation (5)), that hold for any calibration size N and without any assumption at all on the target posterior distribution.

Moreover, Equation (6) shows that $\hat{p}(\theta; \theta^2)$ can be interpreted as a p -value for testing the null hypothesis that θ^2 and θ are drawn iid from Π , since its null distribution is super-uniform. This enables formal hypothesis testing under the posterior, though of a rather different nature from traditional Bayesian procedures such as tests relying on Bayes factors (Jeffreys 1998, Kass & Raftery 1995). The proposed conformal test has a distinctly

frequentist flavor, as it treats the posterior Π as an unknown distribution estimated from iid Monte Carlo samples, and the conformal p -value provides a classical tool to test a nonparametric null hypothesis on the joint distribution of the calibration samples and a hypothetical new draw from Π . More generally, if one prefers not to attach a strict testing interpretation to $\hat{p}(\theta; \theta^2)$, this quantity can still be viewed as a normalized measure of the *typicality* of θ with respect to Π : larger values correspond to parameters that rank higher, under the \mathcal{D} -KDE score, than most calibration samples. Even under this heuristic interpretation, the conformal analysis based on $\hat{p}(\theta; \theta^2)$ offers a more nuanced characterization of the uncertainty encoded in Π than a simple point estimate alone could provide.

An additional appealing feature of the procedure is that it may be applied conditionally on any subregion of Θ with positive posterior mass. This is particularly useful when one wishes to perform inference while fixing certain aspects of the complex parameter. For example, as already mentioned, in clustering applications one may wish to assess posterior uncertainty conditional on partitions with at most three interpretable clusters. In this case, a valid credible region can be constructed from the calibration scores associated with partitions having at most three clusters, with coverage guaranteed relative to the posterior conditioned on the nonzero- Π event of no more than three clusters.

On a final note on Proposition 1, it is well known ([Angelopoulos & Bates 2023](#)) that the coverage guarantee in Equation (4) is independent of the choice of scoring rule, as it relies solely on the exchangeability between calibration and new samples. Nevertheless, the practical utility of the resulting credible region depends critically on this choice. Arbitrary scores may yield overly large regions (since even the whole Θ itself trivially satisfies the guarantee) or exclude high concentration areas if the score misaligns with Π . Designing an informative score is therefore essential. Our distance-based KDE construction offers a principled solution: it exploits (i) the geometry of Θ induced by \mathcal{D} , which helps cap-

ture the structure of the effective posterior support, and (ii) the inherent concentration of training samples in high-probability regions. In our illustrations, we verify empirically that this choice yields credible regions of reasonable size and consistent posterior alignment in practice.

Remark 1. *The concentration inequality in Equation (5) is of independent interest, and its original proof, based on the Dvoretzky–Kiefer–Wolfowitz inequality (Dvoretzky et al. 1956, Massart 1990), can be found in the Supplementary Material. It is in the spirit of existing results (Vovk 2012, Sarkar & Kuchibhotla 2023, Lei et al. 2018) that study the coverage of the conformal set as a random variable conditional on the calibration scores, and establish high-probability bounds for the event of that coverage exceeding $1 - \alpha$. Our inequality goes a step further (under the assumption of iid scores), as it specifies when and at what rate this coverage converges exactly to $1 - \alpha$, rather than merely exceeding it. As already noted, the bound includes a term that may not vanish asymptotically in the presence of atoms in the score distribution; when Π is continuous, however, the inequality simplifies to*

$$|\Pi(\mathcal{C}_{1-\alpha}(\theta^2)) - (1 - \alpha)| \leq \frac{1 + \max(\alpha, 1 - \alpha)}{N} + \sqrt{\frac{1}{2N} \ln\left(\frac{2}{\delta}\right)}$$

with $\mathbb{P}_{\theta^2 \sim \Pi}$ -probability at least $1 - \delta$, implying $O(N^{-1/2})$ concentration around the desired coverage level $1 - \alpha$. For a high-probability guarantee that the coverage merely exceeds $1 - \alpha$, one may instead use the results in the references cited above.

4.1 Connections to metric balls as credible regions

Given a discrepancy \mathcal{D} and a point estimate $\hat{\theta} \in \Theta$, a natural alternative credible set is the \mathcal{D} -ball around $\hat{\theta}$ with radius chosen to achieve (empirical) $1 - \alpha$ posterior coverage. For instance, in Bayesian clustering with the VI metric, this is the standard approach popularized by Wade & Ghahramani (2018). Intriguingly, such credible balls can be recovered within our CBI framework by simply choosing a different scoring rule. Let $\hat{\theta}$ be any estimator

computed from the training sample θ^1 (e.g., the \mathcal{D} -KDE maximizer within θ^1). For each calibration draw, define

$$\tilde{s}(\theta; \theta^1) := -\mathcal{D}(\theta, \hat{\theta}).$$

Standard conformal prediction results (Vovk et al. 2005, Angelopoulos & Bates 2023) then yield the $(1 - \alpha)$ conformal credible region

$$\{\theta \in \Theta : \mathcal{D}(\theta, \hat{\theta}) \leq \hat{q}_{1-\alpha}\},$$

where $\hat{q}_{1-\alpha}$ is the empirical $n^{-1} \lceil (n+1)(1-\alpha) \rceil$ -quantile of $\{\mathcal{D}(\theta, \hat{\theta}) : \theta \in \theta^2\}$. Thus, credible balls emerge as a special case of CBI, but now equipped with the exact, assumption-free posterior coverage guarantees of Theorem 1, rather than simply relying on Monte Carlo validity heuristics.

While this reinterpretation is conceptually useful, we argue that the \mathcal{D} -KDE procedure remains preferable in most applications, unless there is strong reason to believe that the posterior is essentially unimodal around $\hat{\theta}$. The intuition behind this is that, on the one hand, our KDE-based conformity score aggregates individual distances to the training samples, so a parameter value receives a relatively high score whenever it is close to *any* of the modes. This allows the resulting conformal set to track the different high-density regions of the posterior: it can reach several separated modes without having to include the low-density “valleys” between them. On the other hand, a ball centered at a single estimate $\hat{\theta}$ (say, the main mode) must “expand in all directions” until it captures the desired fraction of calibration draws. If the posterior is multimodal, this may have two undesirable consequences. First, to reach the secondary modes it must expand through the low-density regions separating them from $\hat{\theta}$. Second, large portions of the parameter space that are far from all modes may be included, simply as an artifact of the fact that the ball radius must grow uniformly in all directions away from $\hat{\theta}$ until coverage is reached. In either case, the resulting credible set will be unnecessarily large and include areas of the parameter space

that are not representative of the posterior support.

Figure 2 illustrates these points with a one-dimensional continuous distribution. The credible sets centered at either the sample mean or the KDE mode become unnecessarily large: both include the low-density region between the modes, and the set centered at the KDE mode extends far to the left of both modes. The KDE-based conformal set, by contrast, adapts perfectly to the multimodal distribution and excludes the unrepresentative areas. Example 2 below shows that these phenomena persist in the substantially more complex space of data partitions.

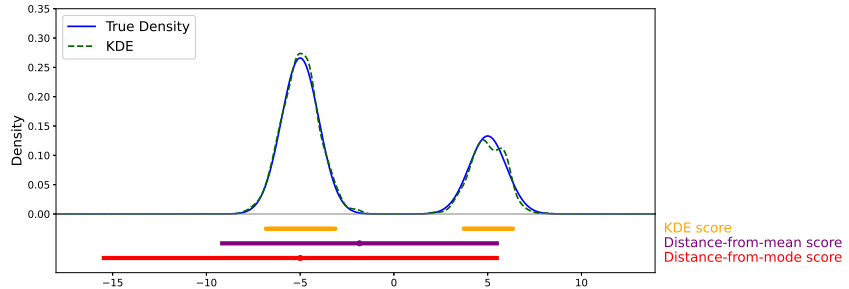


Figure 2: One-dimensional illustration comparing the KDE-based credible set with Euclidean balls centered at point estimates (all with 90% coverage). The KDE-based set adapts to multimodality, whereas ball-type sets include large low-density regions.

4.2 Theoretical justification of iid assumption

In this subsection, we provide theoretical justification for the iid assumption on the calibration scores. Before doing so, we observe that even if this assumption fails, one can still attach probabilistic guarantees to the coverage achieved by $\mathcal{C}_{1-\alpha}(\theta^2)$. Indeed, because the ordering of the calibration scores plays no role in constructing the credible region, we may without loss of generality randomly shuffle them and regard the resulting sequence as exchangeable. Since exchangeability is precisely the condition required for the conformal guarantees to hold, the marginal coverage guarantee in Equation (4) continues to apply,

with the iid assumption replaced by the corresponding exchangeable law for the calibration and new samples. The interpretation of the guarantee as a statement about the expected posterior coverage changes accordingly, as does the null hypothesis under which the quantity in Equation 2 is formally a p -value.⁸ Nevertheless, to maintain a cleaner and more interpretable connection between the theoretical guarantees and the outputs of our procedure, it is valuable to establish conditions under which the calibration sample may indeed be viewed as iid even when it is generated from MCMC, which we tackle next.

Recall that we collect $N := T - S$ calibration samples. For simplicity, re-index them as $\theta_0, \theta_M, \dots, \theta_{M(N-1)}$, where M acts as a thinning parameter determining which samples are included in the calibration set (that is, every M th element from the original sample is retained). While the iid assumption is crucial for obtaining a valid credible region under conformal prediction principles, in practice we often have access not to iid samples from Π , but to Markov-dependent samples produced by an MCMC algorithm. However, such a sampler is typically designed to be Π -mixing, meaning that $\lim_{t \rightarrow \infty} \sup_{\theta_0 \in \Theta} \|\mathcal{L}_t(\cdot | \theta_0) - \Pi\|_{TV} = 0$, where $\mathcal{L}_t(\cdot | \theta_0)$ denotes the distribution of θ_t conditional on the chain starting at θ_0 , and $\|\cdot\|_{TV}$ denotes the total variation (TV) distance between probability measures. Recall that, for two probability measures μ and ν on a sample space Ω , the TV distance is defined as

$$\|\mu - \nu\|_{TV} := \frac{1}{2} \sup_{A \subseteq \Omega} |\mu(A) - \nu(A)| = \frac{1}{2} \sup_{h \in [-1, 1]^\Omega} \left| \int_{\Omega} h \, d\mu - \int_{\Omega} h \, d\nu \right|.$$

Under stronger assumptions, one can sometimes establish quantitative convergence, i.e., that the chain is Π -mixing at rate ε_t , meaning that $\sup_{\theta_0 \in \Theta} \|\mathcal{L}_t(\cdot | \theta_0) - \Pi\|_{TV} \leq \varepsilon_t$, for some decreasing sequence $(\varepsilon_t)_{t \in \mathbb{N}}$; see [Levin & Peres \(2017\)](#) for a standard and comprehensive treatment.

⁸The high-probability guarantee in Equation 4 can also be adapted, although doing so requires additional care.

The following result shows that, as long as the chain is mixing, the joint law of the calibration scores $(s_0, s_M, \dots, s_{M(N-1)})$ computed from a suitably thinned calibration sample $(\theta_0, \theta_M, \dots, \theta_{M(N-1)})$, approaches that of a posterior iid vector in TV distance (as $M \rightarrow \infty$).

Proposition 2. *Let $M, N \in \mathbb{N}$, let μ denote the posterior score distribution, $\mu_{N,M}$ the joint law of $(s_0, s_M, \dots, s_{M(N-1)})$, and $\mu^{(N)}$ the N -fold product of μ . If the Markov chain $(\theta_t)_{t \geq 0}$ is Π -mixing and started in stationarity ($\theta_0 \sim \Pi$), then*

$$\lim_{M \rightarrow \infty} \|\mu_{N,M} - \mu^{(N)}\|_{TV} = 0.$$

Moreover, if the chain is Π -mixing at rate ε_t , then

$$\|\mu_{N,M} - \mu^{(N)}\|_{TV} \leq (N-1)\varepsilon_M. \quad (7)$$

In practice, Proposition 2 ensures that, even if the sampled parameters are Markov dependent,⁹ appropriate thinning allows one to treat them as effectively iid. In fact, if the chain is Π -mixing at rate ε_t , one can even choose the spacing M to achieve a desired coverage level in light of Proposition 1: by the definition of the TV distance in terms of bounded test functions, Proposition 2 implies that selecting M large enough ensures an expected value of $\Pi(\mathcal{C}_{1-\alpha}(\theta^2))$ close to $1 - \alpha$ (as $\theta^2 \mapsto \Pi(\mathcal{C}_{1-\alpha}(\theta^2))$ is bounded by 1). Similarly, using the set-based definition of TV distance, one can tune M to obtain an approximate high-probability coverage statement.

We conclude this discussion by noting that the linear dependence on N of the bound in Equation (7) arises from a rather crude argument that treats the calibration samples as

⁹Notice that, in our random partition application, the MCMC algorithm operates on a higher-dimensional space than Θ (i.e., including mixture parameters in addition to the data partition). The resulting chain is then Markov on this larger space, but not necessarily when projected on Θ . This does not affect Proposition 2, since the scores can be viewed as functions from the higher-dimensional state space to the real line. For simplicity, however, we state the result assuming the chain is defined directly on Θ .

ordered and thus Markov dependent. In practice, however, we have already shown that the scores may be seen as exchangeable for the purposes of building $\mathcal{C}_{1-\alpha}(\theta^2)$. From this viewpoint, a larger N can even improve the TV bound, since shuffling more samples tends to reduce dependence more effectively. We do not pursue this refinement further, as it adds little methodological insight beyond the main point that, after appropriate thinning and burn-in, the calibration samples can be safely regarded as iid draws from the target posterior distribution.

Example 2. Consider the simulated data and MCMC output analyzed in Example 1. Based on the \mathcal{D}_{VI} -KDE calibration scores, we construct the credible set $\mathcal{C}_{0.9}(\theta^2)$. To assess its properties, we test whether the following partitions belong to it: (i) the true data partition shown in Figure 1a; (ii) the same (collapsed) partition with the two leftmost clusters merged; (iii) 1,000 randomly generated partitions, each drawn independently by first sampling K from the empirical posterior distribution of the number of clusters (cf. Figure 1b), and then assigning each observation to one of K clusters uniformly at random.

We find that both partitions in (i) and (ii) are contained in the set. Given the point estimate shown in Figure 1c, the inclusion of the collapsed partition is unsurprising, as it closely resembles that estimate. More interestingly, the true partition itself is also included in the set, even though point estimation alone would not have led us to expect this, since the true and collapsed partitions are quite different. This indicates the presence of posterior uncertainty, likely in the form of multimodality, which we will examine further in the next section. Moreover, none of the 1,000 randomly generated partitions fall within the credible region. This supports the view that the credible set does not achieve high coverage simply by encompassing many arbitrary partitions (e.g., those consistent with the marginal posterior on K but otherwise unstructured), but rather by concentrating on representative regions of the posterior.

As a further demonstration of the reasonable size of our credible set, and as an illustration of the advantages of our \mathcal{D}_{VI} -KDE region over \mathcal{D}_{VI} -balls (centered at the \mathcal{D}_{VI} -KDE point estimate, essentially as proposed by [Wade & Ghahramani \(2018\)](#); cf. Subsection 4.1), we examine how both procedures behave on the two partitions displayed in Figure 3. The partition on the left can be reached by “moving away” from the collapsed partition in the “opposite direction” compared to the true partition (recall that both the true and collapsed partitions lie in our credible set, and in Section 5 below we will show that they practically coincide with the two posterior modes), as it groups into the leftmost cluster of the collapsed partition several observations that clearly belong to the rightmost one. The partition on the right of Figure 3, by contrast, lies “between” the two modes: it shrinks one of the true leftmost clusters of the true partition by reassigning some of its members to the other left cluster, thereby making the partition closer to the collapsed one.

In both scenarios, our \mathcal{D}_{VI} -KDE conformal p -value falls below the 0.1 inclusion threshold, whereas the p -value associated with the credible ball remains above the threshold. This indicates the presence of low-density regions both between and away from the two modes, and while our KDE-based procedure correctly downweights these regions by focusing on the effective support of the posterior, the more crude credible ball unnecessarily includes the two unrepresentative partitions coming from such regions. This behavior is fully consistent with the one-dimensional intuition illustrated earlier in Figure 2.

5 Multimodality analysis

Having defined our approach to point estimation and credible region construction, we now turn to the last piece of the CBI program, that is to address multimodality in the posterior distribution over Θ . Importantly, because the parameter spaces embodied by Θ are generally non-Euclidean, we require a notion of multimodality that is operationally meaningful

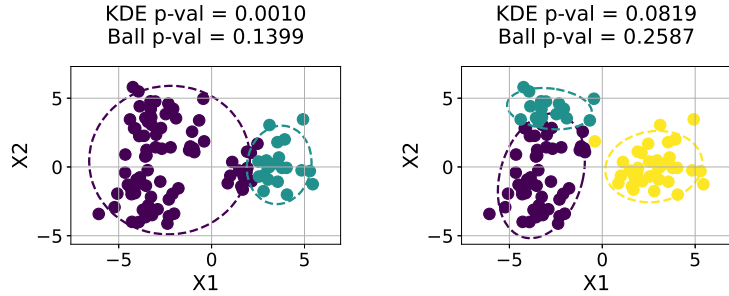


Figure 3: Two partitions tested according to the \mathcal{D}_{VI} -KDE and and \mathcal{D}_{VI} -ball conformal procedures. The partition on the left moves away from the collapsed partition in the opposite direction with respect to the true partition, while the partition on the right lies between the true and collapsed partitions.

within these structures. In particular, we have defined a pseudo-density function, based on the training data, that can be evaluated at any $\theta \in \Theta$, and we can compute a distance $\mathcal{D}(\theta, \theta')$ between any two parameters $\theta, \theta' \in \Theta$. These two ingredients are sufficient to define a concept of multimodality grounded in the idea of *density-based clustering*. The latter provides a general framework, encompassing many algorithmic instantiations (Ester et al. 1996, Kriegel et al. 2011, Rodriguez & Laio 2014), based on the following principle: given a notion of density¹⁰ on Θ and a measure of discrepancy between its elements, one partitions the data into clusters such that (a) each cluster lies in a high-density region whose elements are mutually close, and (b) points from different clusters are far apart. A distribution is then said to be multimodal if random samples drawn from it fall into more than one cluster.

Among the many algorithms following this idea, we take inspiration from the Density Peak Clustering (DPC) procedure by Rodriguez & Laio (2014), which is simple, computationally

¹⁰The term “density” is somewhat ambiguous in this context, as it may refer either to a notion of local concentration of mass (or sampled points) or, relatedly when applicable, to the probabilistic concept of a density as a Radon–Nikodym derivative with respect to a dominating measure. In our setting, the former interpretation is the most appropriate.

efficient, and well suited to our setting. In particular, since the construction of the credible region already requires the N \mathcal{D} -KDE calibration scores to build the credible set, this algorithm can be applied with minimal additional computation. The only remaining step is to compute the pairwise distances $\mathcal{D}(\theta, \theta')$ between all distinct calibration samples θ, θ' ; this has $O(N^2)$ cost, but is parallelizable across each distance computation. Then our procedure, which we term KDE-DPC, proceeds as follows:

1. For each calibration parameter $\theta \in \theta^2$, compute

$$\delta(\theta) := \min_{\theta' \in \theta^2 : s(\theta'; \theta^1) > s(\theta; \theta^1)} \mathcal{D}(\theta, \theta'),$$

that is, the minimum distance from θ to any other parameter with higher density.

For the parameter(s) with highest density (corresponding to our point estimate θ_*), set by default

$$\delta(\theta_*) := \max_{\theta' \in \theta^2} \mathcal{D}(\theta_*, \theta').$$

2. Identify the potential cluster centers as those calibration parameters exhibiting simultaneously high density $s(\theta; \theta^1)$ and large separation $\delta(\theta)$.
3. Optionally, assign each calibration parameter θ to the cluster with the nearest center.

We note that, if one were to follow [Rodriguez & Laio \(2014\)](#) exactly, the density for each calibration sample θ would instead be estimated as the proportion of samples within a fixed-radius \mathcal{D} -neighborhood of θ . While feasible, this would waste computation, since the KDE scores have already been computed, and it would ignore the information contributed by the training samples θ^1 . Nevertheless, the overall approach is retained, as the \mathcal{D} -KDE remains distance-based, with the exponential kernel acting as a smoother version of a strict neighborhood.

The KDE-DPC procedure exhibits several appealing features. First, as illustrated in [Example 3](#), the selection of representative parameter values corresponding to posterior modes

reduces to a simple visual task: inspecting a decision graph where, for each calibration sample θ , the quantities $\delta(\theta)$ (on the vertical axis) and $s(\theta; \theta^1)$ (on the horizontal axis) are plotted. The posterior modes are then identified as those samples that stand out as having abnormally large values of both quantities—that is, points lying in the north-east corner of the decision graph. This approach has the practical advantage of not requiring a pre-specified the number of modes, which is instead discovered together with the modes themselves. Second, the posterior weight associated with each mode can be naturally estimated as the proportion of calibration samples assigned to its cluster. Third, the method provides a straightforward way to classify calibration samples as inliers or outliers: samples lying in the north-west corner of the decision graph can be interpreted as outliers, since they are far from higher-density samples yet have low density themselves, while those located in the middle and south-east regions are inliers, as they exhibit moderate to high density and are close to representative modes. These considerations significantly enhance one's understanding of the uncertainty encoded by the posterior distribution.

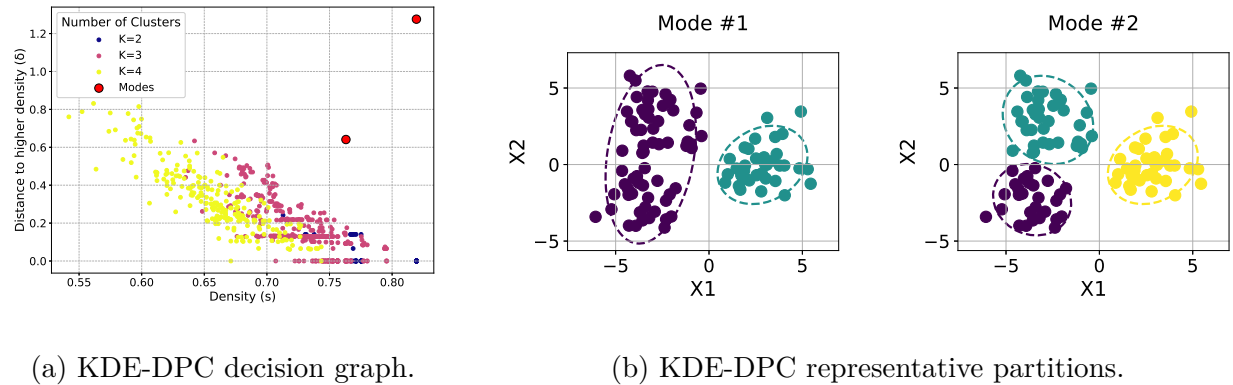
Example 3. *We continue our analysis of the MCMC samples of random partitions introduced in Examples 1 and 2. Figure 4a displays the KDE-DPC decision graph, plotting for each calibration partition its separation δ and density $s(\cdot; \theta^1)$ values, with points colored by the number of clusters in the corresponding partition.¹¹ Two points (highlighted in red) clearly stand out in the north-east corner of the graph, identifying the representative modes. The corresponding partitions, shown in Figure 4b (ordered by density from left to right), indicate that the posterior concentrates substantial mass around two distinct configurations: one with two clusters, obtained by merging the two leftmost clusters of the true data partition (coinciding by default with θ_* as found in Example 1), and another nearly identical to the true partition itself.¹²*

¹¹A large number of two-cluster partitions in the calibration set coincide exactly with the partition corresponding to the north-east-most point, which explains the limited number of visible blue points.

¹²See the Supplementary Material for an additional experiment using the same simulated data and a

Interestingly, coloring by the number of clusters reveals that, while the posterior assigns non-negligible mass to partitions with four clusters, none of these emerge as representative modes. Instead, they appear either as inliers close to one of the two main modes (the yellow points at the center of the decision graph) or as outliers lying in low-density regions far from the modes (the yellow points in the north-west area of the decision graph). In this sense, the multimodality analysis suggests that, although four-cluster configurations receive some posterior support under the PY mixture model used to fit the data, they are likely spurious from the standpoint of a parsimonious description of the uncertainty encoded in the posterior distribution.

Figure 4: Multimodality analysis results (Gaussian mixture data, analyzed with a PY Gaussian density mixture model).



To conclude, we note that the output of our multimodality analysis based on the KDE-DPC procedure is analogous to that of [Balocchi & Wade \(2025\)](#), who summarize the posterior over partitions using a Wasserstein-distance-minimizing mixture of point masses at representative partitions. In both approaches, the result is a set of posterior modes capturing meaningfully separated regions of posterior concentration in the partition space. A few advantages of our approach are worth highlighting. First, it only requires density scores (already computed for the credible region) and pairwise VI distances between calibration sam-

similar prior, where the posterior over partitions is instead found to be unimodal.

ples (also required by [Balocchi & Wade \(2025\)](#)), both of which can be parallelized to achieve substantial computational gains. In contrast, the k -medoids-like algorithm of [Balocchi & Wade \(2025\)](#) is inherently sequential. Second, their method requires specifying the number of modes in advance. To select a good value of this important hyperparameter, the authors propose running the algorithm for different choices and picking the one with the largest improvement in posterior approximation. Clearly, this approach may be computationally cumbersome and prone to overfitting to the available MCMC samples. Our KDE-DPC procedure, by contrast, automatically reveals the number of modes through visual inspection of the decision graph. Finally, [Balocchi & Wade \(2025\)](#) propose several insightful techniques to characterize posterior uncertainty once the modes are identified, such as plotting the meet between any two representative partitions or examining the VI contribution of each data point. All of these analyses can naturally be performed using the representative partitions discovered by our KDE-DPC algorithm. Since our main focus is on the broader CBI methodology, and because these tools are thoroughly detailed by [Balocchi & Wade \(2025\)](#), we refer the interested reader to their thoughtful discussion.

6 Real data applications

We are now in a position to illustrate our CBI methodology, in its \mathcal{D}_{VI} -based instantiation for random partition models, as applied to two real-world datasets: the classic Galaxy velocities data ([Roeder 1990](#)) and ERP functional data ([Song et al. 2025, Kappenman et al. 2021](#)).

6.1 Galaxy velocities data

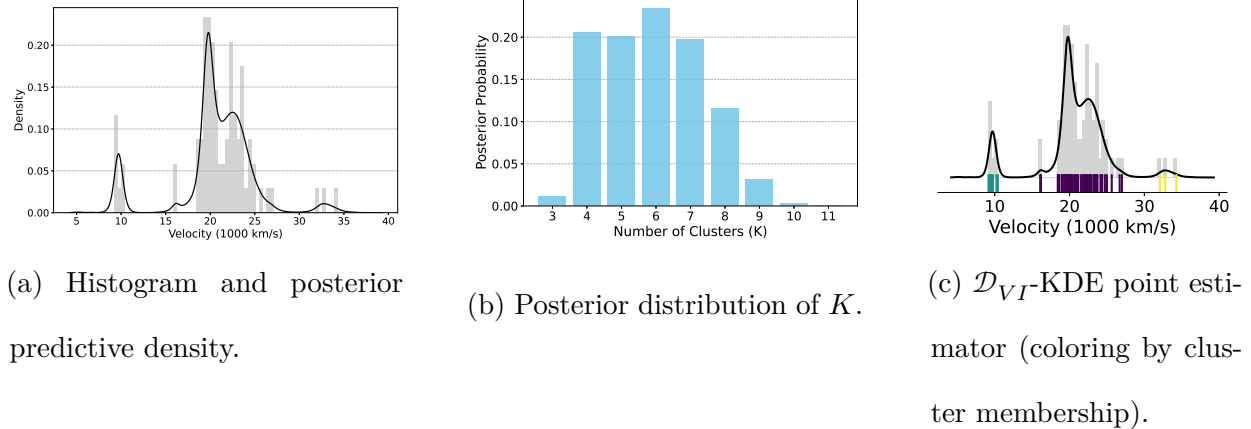
The Galaxy velocities dataset is a well-known and simple benchmark for mixture-based density estimation and clustering. It contains velocity measurements (in units of 1,000

km/second) for 82 galaxies observed in six well-separated conic sections of the Corona Borealis region (Roeder 1990). We analyze this dataset using a Pitman–Yor Gaussian mixture model, fitted via a marginal Gibbs sampler implemented in `pyrichlet` (Selva et al. 2025). For the subsequent CBI analysis, we use 5,000 training and 1,000 calibration MCMC samples after appropriate burn-in and thinning. Figure 5a shows a histogram of the data together with the posterior predictive estimate of the density.

Figure 5b visualizes the estimated posterior distribution of the number of clusters in the data, which is spread over a relatively wide range of values, indicating substantial uncertainty. Figure 5c displays the \mathcal{D}_{VI} -KDE point estimate of the data partition, which reveals three spatially well-separated clusters. At first glance, this may appear inconsistent with the relatively small posterior mass assigned to partitions with three clusters in Figure 5b. However, recall that our point estimation procedure seeks the partition maximizing the \mathcal{D}_{VI} -KDE score. Since this score is constructed using the VI distance, the procedure naturally selects a representative partition that is well supported by the posterior training samples under that distance. Because, as we have already discussed, the very design of \mathcal{D}_{VI} favors more parsimonious partitions, this result is in fact expected and arguably desirable: in the absence of strong prior beliefs supporting the presence of additional clusters, an Occam’s razor principle naturally suggests preferring a simpler clustering representation. This is particularly reasonable if many of the sampled partitions, for example those with four or five clusters, differ only slightly from the selected three-cluster configuration (see also the point coloring in Figure 6a).

The view that the posterior distribution reflects a substantial degree of uncertainty is further supported by the 90% conformal credible set, which we find to include all k -means clusterings with $k = 3, 4, 5, 6$. Additionally, we repeat the size check performed for the simulated data example in the previous section, where we test whether 1,000 randomly

Figure 5: Galaxy velocities dataset clustering experiment (analyzed with a PY Gaussian density mixture model).



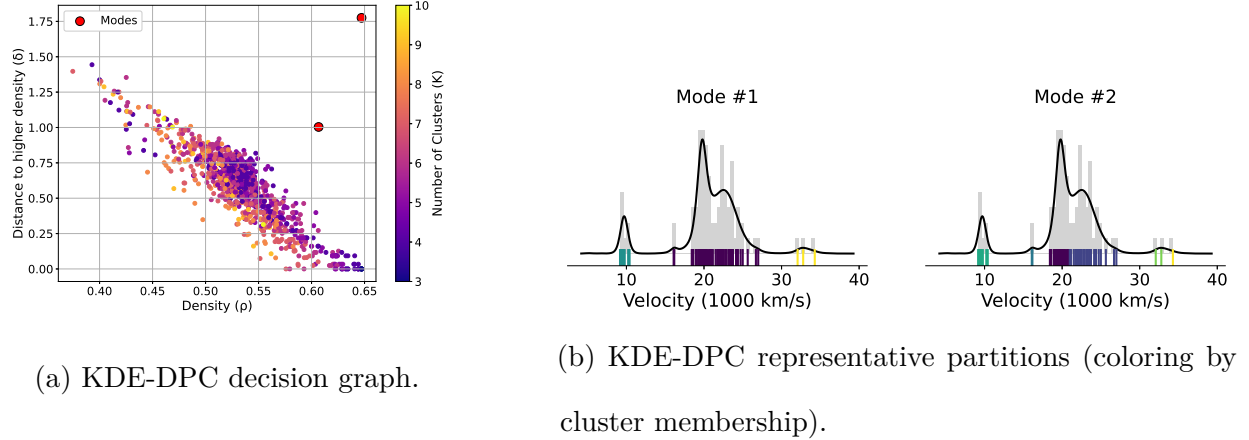
generated partitions fall within the conformal set. The results are encouraging, as none of the randomly generated partitions fall inside the conformal set.

Finally, Figures 6a and 6b report the results from the DPC-based multimodality analysis. As the decision graph clearly shows, two well-separated modes are identified, corresponding to the three-cluster point estimate as well as a six-cluster refinement of it. Both partitions are plausible given the empirical distribution of the data, and the multimodality analysis reveals that both receive support by the posterior distribution over data partitions derived from the adopted Bayesian model.

6.2 ERP data experiment

Our second application of CBI concerns functional data clustering using a specialized Bayesian random partition model. Specifically, we build on the analysis of [Song et al. \(2025\)](#), who employ a projection Determinantal Point Process (pDPP) repulsive mixture prior ([Xu et al. 2016](#), [Xie & Xu 2020](#), [Petralia et al. 2012](#), [Beraha et al. 2025](#), [Cremaschi et al. 2025](#)) to analyze data from the publicly available ERP CORE project ([Kappenman](#)

Figure 6: Multimodality analysis results for the Galaxy velocities data.



et al. 2021). The goal of the analysis is to obtain interpretable clusters of functional data representing ERP waveforms recorded from 34 young adult participants exposed to certain visual stimuli. We refer the reader to Section 7 of Song et al. (2025) for additional scientific context. Figure 7a visualizes the analyzed data in terms of waveform amplitudes measured up to 800 milliseconds after stimulus onset. Song et al. (2025) fit their Bayesian pDPP repulsive mixture model using the first four functional principal components of the data. The employed MCMC algorithm generates posterior samples of the random partition of the 34 subjects, which we use as the input to our CBI analysis.

As shown in Figure 7b, the posterior distribution concentrates around a single representative partition, which corresponds to the \mathcal{D}_{VI} -KDE point estimate in Figure 7c featuring four distinct clusters. Interestingly, this estimate matches that obtained by Song et al. (2025) (see their Figure 5) using the SALSO algorithm (Dahl et al. 2022).

After constructing the 90% credible region from the calibration scores, we test two extreme hypotheses. First, we assess whether the posterior supports full heterogeneity, i.e., the trivial partition with 34 clusters. It does not: the corresponding conformal p -value¹³ equals

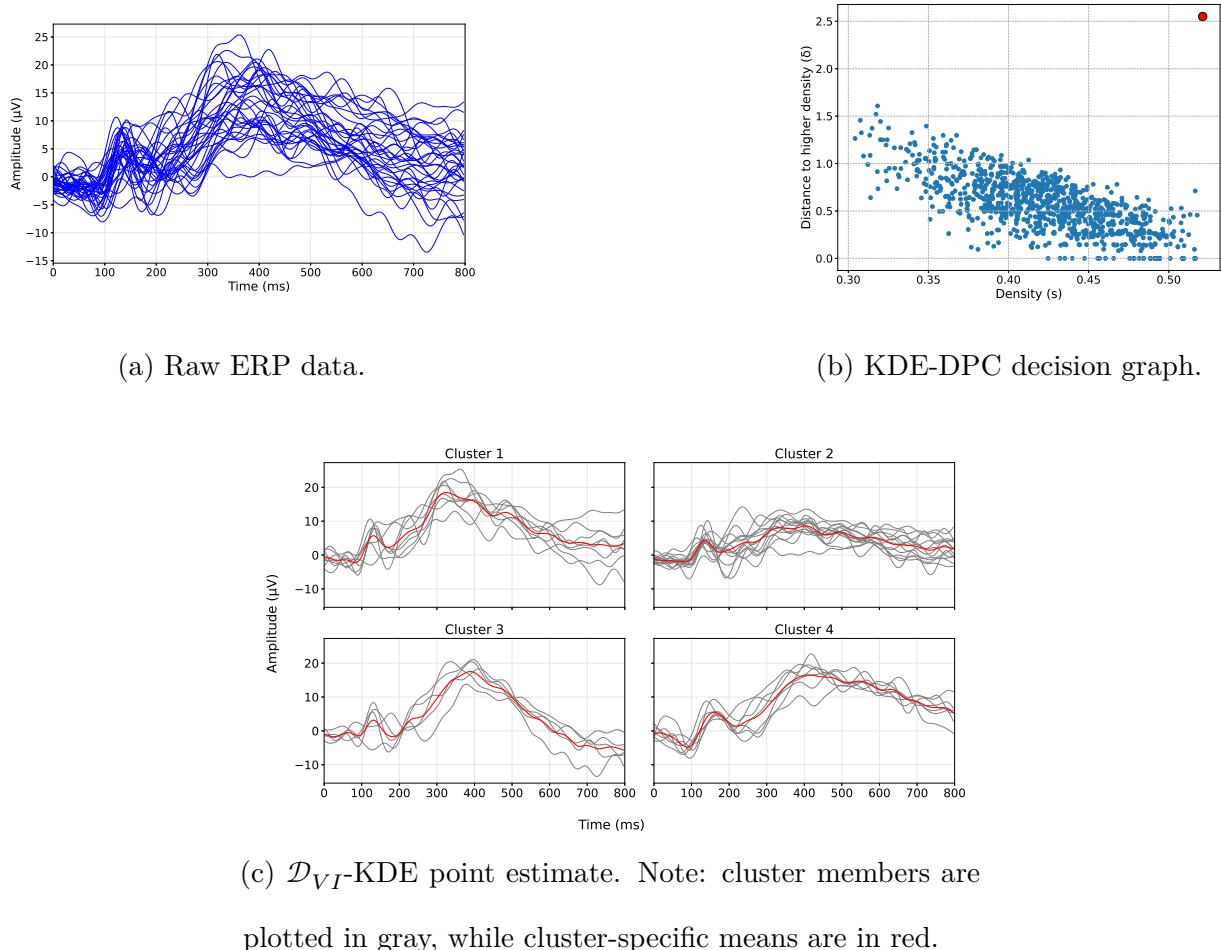
¹³Recall from Equation (6) that $\hat{p}(\theta; \theta^2)$ is a p -value under the null hypothesis $(\theta^2, \theta) \stackrel{\text{iid}}{\sim} \Pi$.

0.000999, indicating that such a configuration is highly atypical under the posterior. This corroborates the finding by [Song et al. \(2025\)](#) that participant subpopulations exhibit meaningful homogeneity. Next, we test whether complete homogeneity (a single cluster) can be rejected as atypical under the posterior. Interestingly, the one-cluster partition is included in the credible set, with conformal p -value equal to 0.140859, indicating that while it is not highly typical, it cannot be decisively ruled out. A robustness check using 1,000 partitions generated uniformly at random confirms that none are included in the credible region, reassuring of the test power. We nevertheless emphasize that this p -value is valid only under the specific null hypothesis that the one-cluster partition is a posterior draw independent of the calibration samples. Even ignoring this formal interpretation, the result should be strictly understood in terms of posterior typicality *under the VI metric*: the \mathcal{D}_{VI} -KDE score blends empirical posterior mass with the VI geometry, implying not that the one-cluster partition is likely (in fact, it never appears among the MCMC samples we use), but that it is not exceedingly atypical relative to posterior samples under the VI metric. More broadly, this null finding provides a good reminder that, while the KDE scoring rule yields a valid credible region with guaranteed posterior coverage by leveraging an informative metric such as \mathcal{D}_{VI} to summarize a complex space like that of partitions, the results of conformal testing should be interpreted strictly within their intended scope.

7 Discussion

This article has introduced Conformalized Bayesian Inference (CBI), a simple, robust and efficient pipeline to turn Monte Carlo samples from a Bayesian posterior distribution on a complex parameter space into interpretable insights about a single representative of that posterior, a posterior credible region based on conformal prediction ideas, and possible posterior multimodalities, all simply requiring a notion of discrepancy between sampled pa-

Figure 7: CBI results for ERP data analyzed using the pDPP mixture model of [Song et al. \(2025\)](#).



rameters. We have explored theoretical and methodological aspects of CBI, and illustrated its power on the notoriously difficult task of inferring the clustering structure of data using Bayesian random partition models. We now turn to a discussion of the limitations of the methodology and what venues for future research are left open.

7.1 Current limitations

Perhaps the most important limitation of CBI is that its usefulness critically depends on the quality of the Monte Carlo samples used in the procedure. While CBI has been shown to effectively summarize samples that are representative of the posterior distribution, this representativeness is essential for obtaining reliable insights about the target posterior. For instance, if the sampler is based on MCMC and has not converged to stationarity, the samples may deviate from the true posterior, leading to biased CBI outputs. Alternatively, in case of poor MCMC mixing, the samples may remain highly dependent even after substantial thinning, which undermines the validity of the conformal credible region. Similarly, if the posterior contains highly disconnected modes and the sampler does not adequately explore them, our multimodality analysis will fail to capture these modes because they are absent from the posterior samples. Therefore, CBI does not remove the need to ensure good performance of the adopted sampler.

Second, although we have shown that the distance-based KDE score is a simple and robust choice for CBI, some posterior distributions may not be well captured by any readily available distance combined with a simple kernel. This limitation could be addressed by developing more flexible pseudo-density estimators, for instance when the parameter space (such as the space of graphs) is suitable for modern deep learning architectures ([Bishop & Bishop 2024](#)).

Finally, we note that the current scope of CBI is limited to a single posterior distribu-

tion. However, much recent work (especially in Bayesian nonparametrics) has focused on dependent priors, and hence dependent posteriors, to model heterogeneous but related populations (MacEachern 2000, Teh et al. 2006, Rodriguez et al. 2008, Lijoi et al. 2014, among many others). A rigorous treatment of dependent posteriors remains an open problem and would substantially extend the applicability of CBI.

7.2 Future directions

The mentioned limitations, together with other considerations, leave a number of important research questions open. In particular, further work is needed to study, both theoretically and empirically, the interplay between the properties of the posterior sampler, the adopted scoring rule, and CBI itself, for instance to understand how these factors jointly affect the size and structure of the conformal credible region. Moreover, multi-sample extensions of CBI would enable its application to dependent observation settings, such as assessing the degree of homogeneity between posteriors arising from dependent priors.

Future research should further investigate the use of CBI on complex parameter spaces beyond partitions, such as graphs, matrices, regression functions, and mixing measures. As noted earlier, we provide preliminary empirical illustrations in the Supplementary Material for cases where Θ represents either the space of mixing measures in mixture models (where \mathcal{D} coincides with the Wasserstein-1 metric), or the space of covariance matrices (discrepancies being measured according to the operator norm) in covariance estimation problems. Additional methodological developments are also of interest, including the integration of alternative density-based clustering methods (Ester et al. 1996, Wang et al. 2019), which could offer a more refined characterization of posterior multimodality—distinguishing, for example, whether the identified representative parameters correspond to distinct high posterior-mass regions separated by low-mass areas, or instead belong to a

single, spread-out region of posterior concentration.

SUPPLEMENTARY MATERIAL

7.3 Proof of Proposition 1

Equations (4) and (6) in the main text are classic results in conformal prediction. Hence, we omit their proof and refer the reader to classic references such as [Vovk et al. \(2005\)](#), [Angelopoulos & Bates \(2023\)](#). Instead, we prove the concentration inequality in Equation (5).

Step 1. The inclusion criterion for the credible region is equivalent to $s(\theta; \theta^1) \geq s_{(k)}$, where $s_{(k)}$ is the k -th order statistic of the calibration scores and $k = \lceil \alpha(N+1) - 1 \rceil$. Let $\Pi_s(s) := \Pi(\{\theta \in \Theta : s(\theta; \theta^1) \leq s\})$ denote the posterior CDF of the scores. The posterior mass of the random credible set is precisely

$$\Pi(\mathcal{C}_{1-\alpha}(\theta^2)) = 1 - \Pi(\{\theta : s(\theta; \theta^1) < s_{(k)}\}) = 1 - \Pi_s(s_{(k)}^-),$$

where the minus sign denotes a left-hand limit. The quantity to be bounded is therefore $|\Pi(\mathcal{C}_{1-\alpha}(\theta^2)) - (1 - \alpha)| = |\alpha - \Pi_s(s_{(k)}^-)|$.

Step 2. For any $\delta \in (0, 1)$, the DKW inequality ([Dvoretzky et al. 1956](#), [Massart 1990](#)) gives

$$\mathbb{P}_{\theta^2 \stackrel{\text{iid}}{\sim} \Pi} \left(\sup_{s \in \mathbb{R}} |\hat{\Pi}_{s,N}(s) - \Pi_s(s)| \leq \epsilon_N(\delta) \right) \geq 1 - \delta,$$

where $\epsilon_N(\delta) = \sqrt{\frac{1}{2N} \ln(\frac{2}{\delta})}$. This implies that, on the same high-probability event, the bound also holds for the left-hand limits: $|\hat{\Pi}_{s,N}(s^-) - \Pi_s(s^-)| \leq \epsilon_N(\delta)$ for all s .

Step 3. The total deviation is bounded using the triangle inequality:

$$|\alpha - \Pi_s(s_{(k)}^-)| \leq \left| \alpha - \frac{k}{N} \right| + \left| \frac{k}{N} - \hat{\Pi}_{s,N}(s_{(k)}^-) \right| + |\hat{\Pi}_{s,N}(s_{(k)}^-) - \Pi_s(s_{(k)}^-)|.$$

Each of the three terms on the right-hand side is now bounded.

1. *Deterministic term:* The definition of k implies $\alpha(N+1) - 1 \leq k < \alpha(N+1)$, which gives the bound:

$$|\alpha - k/N| \leq \frac{\max(\alpha, 1 - \alpha)}{N}.$$

2. *Empirical jump size:* The term $|\frac{k}{N} - \hat{\Pi}_{s,N}(s_{(k)}^-)|$ represents the proportion of samples with scores exactly equal to $s_{(k)}$. This is because $\hat{\Pi}_{s,N}(s_{(k)}^-) = \frac{1}{N}|\{t : s(\theta_t; \theta^1) < s_{(k)}\}|$. If m samples have a score of $s_{(k)}$, then there are $k - m$ scores strictly less than $s_{(k)}$, so $\hat{\Pi}_{s,N}(s_{(k)}^-) = (k - m)/N$. The term thus equals m/N . In the absence of ties ($m = 1$), this term is $1/N$, so it vanishes deterministically if the posterior distribution of the scores is continuous.

3. *DKW Error:* From Step 2, with probability at least $1 - \delta$, this stochastic term is bounded by:

$$|\hat{\Pi}_{s,N}(s_{(k)}^-) - \Pi_s(s_{(k)}^-)| \leq \epsilon_N(\delta).$$

Step 4. Combining the bounds for the three terms yields the final inequality.

7.4 Proof of Proposition 2

We show a proof of the second, quantitative statement, which readily implies a proof of the first asymptotic property. The proof proceeds via the dual representation of the total variation distance:

$$\|\mu_{N,M} - \mu^{(N)}\|_{TV} = \frac{1}{2} \sup_{h \in [-1,1]^{\mathbb{R}^N}} |\mathbb{E}[h(s)] - \mathbb{E}[h(s')]|,$$

where $s = (s_0, s_M, \dots, s_{M(N-1)})$ is the vector of scores derived from the thinned Markov chain, with $s_{Mk} = f(\theta_{Mk})$ for a measurable scoring function f , and $s' = (s'_0, \dots, s'_{N-1})$ is a vector of scores derived from an independent and identically distributed sequence of parameters $(\theta'_0, \dots, \theta'_{N-1})$ from Π .

For $k = 0, \dots, N-1$, define a hybrid sequence of parameters $\vec{\theta}^{(k)} = (\theta_0^{(k)}, \dots, \theta_{M(N-1)}^{(k)})$.

The law of this sequence is constructed as follows: the initial state θ_0 is drawn from Π ; for $j = 1, \dots, k$, the parameter θ_{Mj} is drawn from the law given by the M -step Markov transition kernel $\mathcal{L}_M(\cdot \mid \theta_{M(j-1)})$; for the remaining steps, $j = k+1, \dots, N-1$, the parameters θ_{Mj} are drawn independently from Π . Let $E_k[h]$ be the expectation of h applied to the scores derived from $\vec{\theta}^{(k)}$. Note that $E_{N-1}[h] = \mathbb{E}[h(s)]$ and $E_0[h] = \mathbb{E}[h(s')]$.

Then, telescoping, we get

$$\mathbb{E}[h(s)] - \mathbb{E}[h(s')] = E_{N-1}[h] - E_0[h] = \sum_{k=1}^{N-1} (E_k[h] - E_{k-1}[h]).$$

Consider a single term $\Delta_k = E_k[h] - E_{k-1}[h]$. The laws generating these two expectations differ only in the distribution of the k -th parameter, θ_{Mk} . Let $\vec{\theta}_{<k} = (\theta_0, \dots, \theta_{M(k-1)})$ and define the function h_k by taking the conditional expectation of h over the subsequent independent parameters:

$$h_k(x; \vec{\theta}_{<k}) = \mathbb{E}_{\theta'_{M(k+1)}, \dots, \theta'_{M(N-1)} \stackrel{\text{iid}}{\sim} \Pi} [h(f(\theta_0), \dots, f(\theta_{M(k-1)}), f(x), f(\theta'_{M(k+1)}), \dots, f(\theta'_{M(N-1)}))].$$

Since $h \in [-1, 1]^{\mathbb{R}^N}$, it follows that $h_k : \Theta \rightarrow [-1, 1]$. The difference Δ_k can then be expressed as:

$$\Delta_k = \mathbb{E}_{\vec{\theta}_{<k}} [\mathbb{E}_{\theta_{Mk} \sim \mathcal{L}_M(\cdot \mid \theta_{M(k-1)})} [h_k(\theta_{Mk}; \vec{\theta}_{<k})] - \mathbb{E}_{\theta_{Mk} \sim \Pi} [h_k(\theta_{Mk}; \vec{\theta}_{<k})]].$$

For any fixed history $\vec{\theta}_{<k}$, the inner term is a difference of expectations bounded by the TV distance between the corresponding measures:

$$\sup_{\theta_{M(k-1)}} \left| \mathbb{E}_{\mathcal{L}_M(\cdot \mid \theta_{M(k-1)})} [h_k] - \mathbb{E}_{\Pi} [h_k] \right| \leq 2 \sup_{\theta_{M(k-1)}} \left\| \mathcal{L}_M(\cdot \mid \theta_{M(k-1)}) - \Pi \right\|_{TV} \leq 2\varepsilon_M.$$

Since this bound does not depend on the history, taking the outer expectation yields $|\Delta_k| \leq 2\varepsilon_M$. Summing the bounds for each term in the telescoping series gives:

$$|\mathbb{E}[h(s)] - \mathbb{E}[h(s')]| \leq \sum_{k=1}^{N-1} |\Delta_k| \leq \sum_{k=1}^{N-1} 2\varepsilon_M = 2(N-1)\varepsilon_M.$$

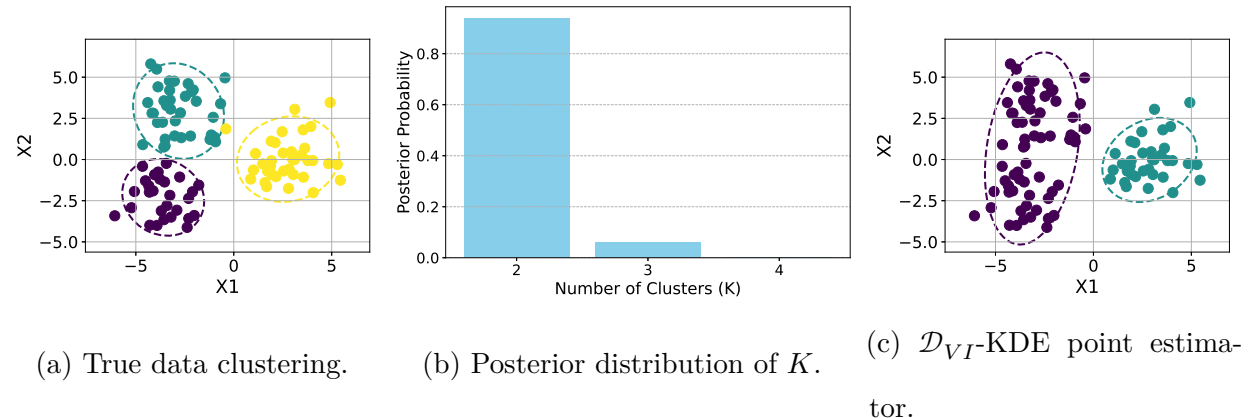
Substituting this into the dual formulation for the total variation distance completes the proof:

$$\|\mu_{N,M} - \mu^{(N)}\|_{TV} = \frac{1}{2} \sup_h |\mathbb{E}[h(s)] - \mathbb{E}[h(s')]| \leq \frac{1}{2} \cdot 2(N-1)\varepsilon_M = (N-1)\varepsilon_M.$$

8 Additional experiment 1: unimodal posterior distribution over partitions

We run a Bayesian clustering experiment analogous to the one used to illustrate CBI in the main text, using the same simulated two-dimensional dataset (Figure 8a). The only difference is that the Pitman-Yor (PY) Gaussian mixture prior is now specified with a smaller concentration parameter, set to 0.01. As is well known (De Blasi et al. 2013), lowering this parameter increases prior mass on partitions with fewer clusters. This shift is reflected in the posterior over the number of clusters K , which becomes more concentrated on small values. Consistent with this, the \mathcal{D}_{VI} -KDE point estimate remains the same two-cluster configuration identified in the example with higher concentration parameter (Figures 8b and 8c).

Figure 8: Gaussian mixture simulated data, analyzed using a PY(0.01, 0.01) Gaussian mixture prior.



(a) True data clustering.

(b) Posterior distribution of K .

(c) \mathcal{D}_{VI} -KDE point estimator.

When constructing the conformal credible region with 90% coverage, we find that it includes the “true partition” when the two leftmost clusters are merged, but no longer the original three-cluster partition. The credible set nevertheless passes the size diagnostic based on 1,000 randomly generated partitions whose number of clusters follows the posterior distribution of K : none of these random partitions fall inside the credible region. Finally, the multimodality analysis in Figure 9 confirms that, under this posterior—corresponding to a prior favoring fewer clusters—the true three-cluster configuration ceases to be a posterior mode, leaving the point estimate as the only identified representative.

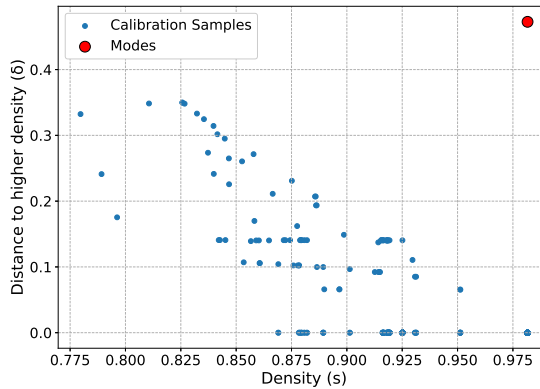


Figure 9: KDE-DPC decision graph (unimodal PY Gaussian mixture posterior on simulated data).

9 Additional experiment 2: Colorectal cancer spatial transcriptomics data (dependent posterior distributions over partitions)

In a recent study, [Duan et al. \(2025\)](#) analyze spatial transcriptomics data on colorectal cancer ([Lee et al. 2020](#)), with the aim of discovering spatially aligned subpopulations of tumor, immune, and stromal cells. Spatial alignment refers to the spatial co-localization of clusters across cell types, where spatial coordinates correspond to the two-dimensional

positions of cells within a medical image. To capture this structure, the authors propose a spatially-aligned random partition model that combines a PY Gaussian mixture model for gene expression features with a prior dependence structure that induces spatial co-localization in the latent clustering across cell types. Their MCMC output consists of sampled partitions for each cell type: cells of different types are clustered separately, but the partitions are modeled as dependent through prior-induced spatial alignment. The results of their analysis indeed reveal subpopulations (clusters) of cells from different types that are spatially co-localized.

We apply our CBI pipeline to these MCMC samples using the VI metric between partitions. For simplicity, we restrict attention to tumor and immune cells only. Figure 10 shows the KDE-DPC decision graphs for the marginal posterior distributions over partitions of both cell types. In both cases, the posterior appears unimodal, indicating that the only meaningful partitions summarizing these posteriors are the point estimates presented next.

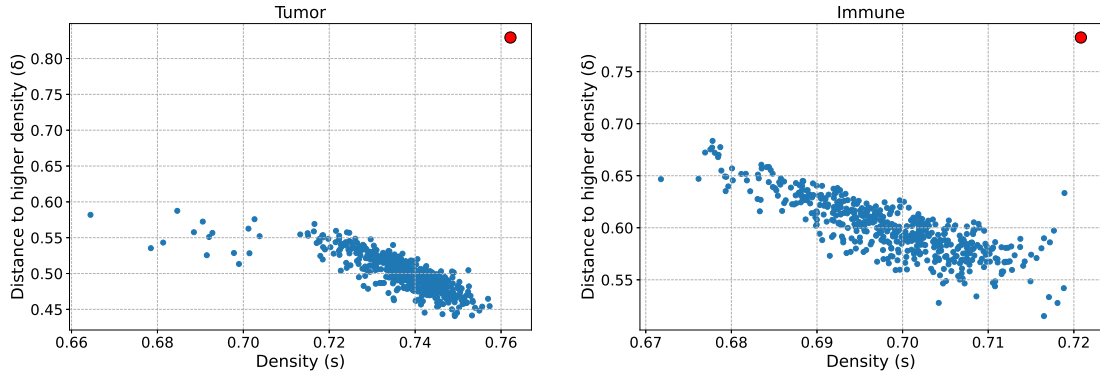


Figure 10: KDE-DPC decision graphs for posterior distributions over partitions of tumor and immune cells.

The left-hand side plots in Figure 11 show the \mathcal{D}_{VI} -KDE point estimates for tumor and immune cell partitions. Recall that the model of [Duan et al. \(2025\)](#) performs density estimation and clustering on high-dimensional gene expression features while using spatial coordinates to induce alignment. For visualization purposes, we display partitions only

in the spatial domain, since spatial alignment is the focus of the analysis. Both point estimates reveal spatially coherent clusters, in line with the findings of [Duan et al. \(2025\)](#).

Finally, we use the conformal credible regions (constructed separately for both marginal posteriors) to test a hypothesis of *global spatial alignment* between the partitions of different cell types. Specifically, given the point estimate for type A cells (either tumor or immune), we spatially translate it to type B cells by matching each type B cell to its closest (spatially) type A cell, and assigning that type B cell to the cluster of the matched type A cell. The right-hand side plots in Figure 11 illustrate these translated partitions. We then check whether each translated partition of type B cells lies within the 90% conformal credible region for the posterior distribution over partitions of type B cells. We emphasize that this constitutes a test of global alignment, as it requires the entire translated partition to lie within the credible region. This is distinct from the goal of [Duan et al. \(2025\)](#), who adopt a more local notion of alignment seeking to identify subsets of clusters that are spatially co-located, rather than assuming full alignment across all clusters. As a result of our analysis, both spatially translated partitions fall outside the corresponding credible regions, supporting the hypothesis that only subsets of tumor and immune cell clusters are spatially co-located. This is consistent with the findings of [Duan et al. \(2025\)](#).

10 Additional experiment 3: posterior distribution over mixing measures

In this experiment, we apply CBI to infer the mixing measure in a Gaussian mixture model. We use again the Galaxy velocities dataset and analyze it as in the main text under the same PY Gaussian mixture model with unchanged prior hyperparameters. The model for

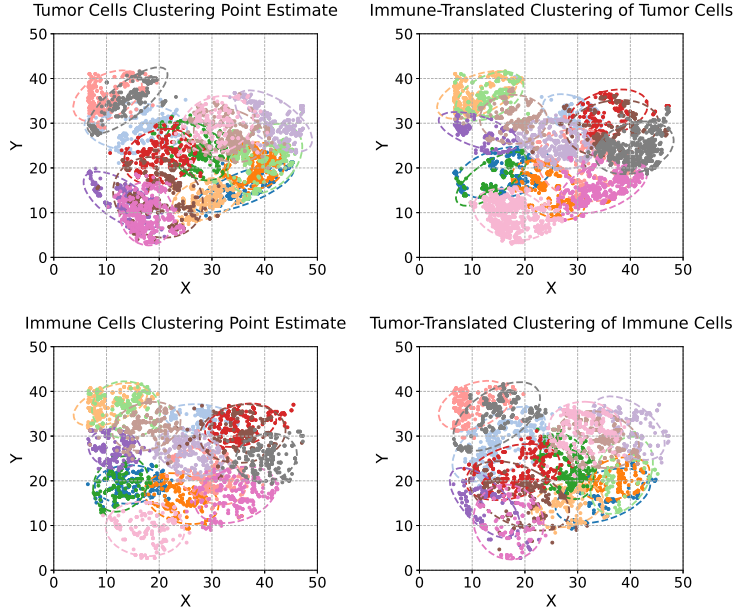


Figure 11: Left: \mathcal{D}_{VI} -KDE point estimates for tumor and immune cell partitions. Right: partitions obtained by spatially translating the \mathcal{D}_{VI} -KDE point estimates across cell types.

the observations X_1, \dots, X_n is

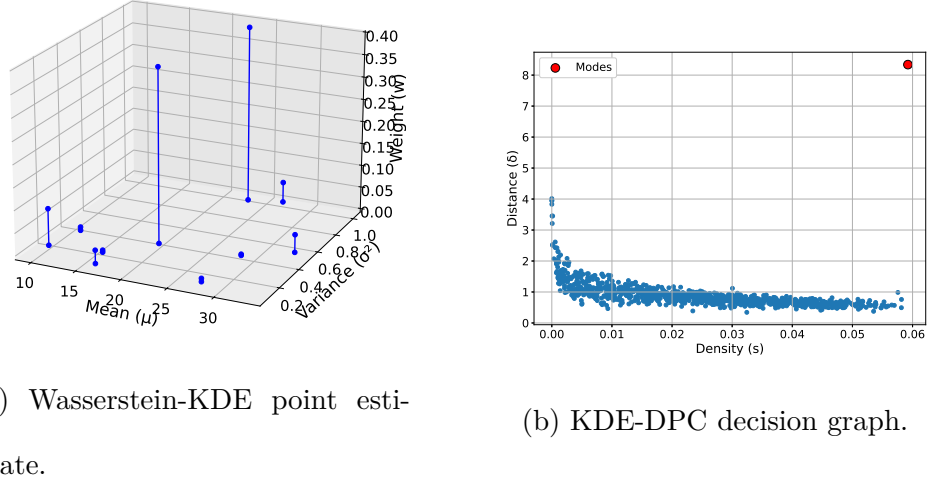
$$X_i \mid \tilde{P} \stackrel{\text{iid}}{\sim} \int_{\mathbb{R} \times \mathbb{R}_+} N(\cdot \mid \mu, \sigma^2) \tilde{P}(d\mu, d\sigma^2),$$

where $N(\cdot \mid \mu, \sigma^2)$ denotes a Gaussian density with mean μ and variance σ^2 , and \tilde{P} is a random probability measure on the space of means and variances endowed with a PY process prior (Perman et al. 1992, Pitman & Yor 1997). Both the prior and posterior distributions of \tilde{P} place their mass on discrete measures with countably many atoms. When appropriate conditional sampling methods are employed (Papaspiliopoulos & Roberts 2008, Walker 2007, Kalli et al. 2011), posterior samples of \tilde{P} can be obtained directly.

Since the Gibbs sampler used in the clustering experiment of the main text marginalizes out \tilde{P} via latent cluster assignments, we refit the model using the conditional sampler implemented in `numpyro` (Phan et al. 2019, Bingham et al. 2019), which employs the NUTS algorithm (Hoffman et al. 2014). We apply the CBI pipeline to 5,000 training and 1,000 calibration samples from the posterior distribution of \tilde{P} , truncated to 10 atoms. Distances

between mixing measures are computed using the Wasserstein-1 distance (Villani et al. 2008, Nguyen 2013), implemented in the `pot` library (Flamary et al. 2021, 2024).

Figure 12: CBI applied to posterior samples of mixing measures (Galaxy velocities dataset analyzed with a PY Gaussian mixture model).



Figures 12a and 12b show that the posterior concentrates around a single mixing measure, which is in line with the empirical distribution of the observed velocities. The 90% conformal credible region contains the empirical k -means mixing measures with $k = 4, 5, 6$, but excludes that with $k = 3$.¹⁴ Compared with the analysis in the main text, where a three-cluster configuration was the highest-KDE point estimate under the VI distance on partitions, this result suggests a subtle distinction: while three clusters best summarize the posterior over partitions, more than three nonzero components are required for the corresponding mixing measure, and hence the implied density, to be plausible under the posterior. This provides a refined understanding of the posterior structure captured by the fitted Bayesian model.

¹⁴The region also passes a basic size check performed by verifying whether 1,000 mixing measures randomly generated according to the prior are included in the region—none of them is.

11 Additional experiment 4: posterior distribution over covariance matrices

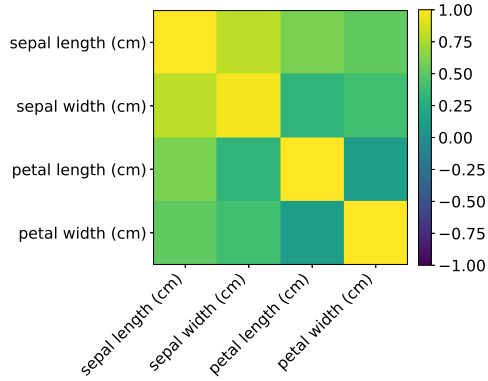
Our final additional experiment applies CBI to covariance estimation. We consider the four-dimensional Iris dataset (Anderson 1936), restricted to the *Setosa* species. After standardizing the observations X_1, \dots, X_n , we fit a simple Gaussian model of the form

$$X_i \mid \Sigma \stackrel{\text{iid}}{\sim} N(\cdot \mid 0, \Sigma),$$

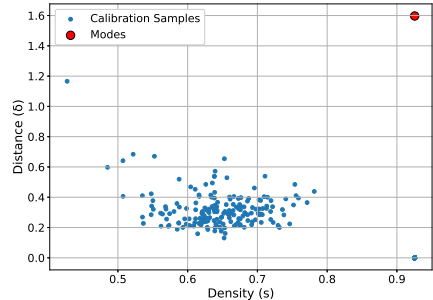
with an LKJ prior on the correlation matrix (Lewandowski et al. 2009). We draw 5,000 training and 1,000 calibration posterior samples for Σ using `numpyro`, and apply CBI by measuring distances between covariance matrices according to the operator norm

$$\|\Sigma\|_{\text{op}} := \max_{v: \|v\|=1} \|\Sigma v\|.$$

Figure 13: CBI applied to posterior samples of covariance matrices (Iris dataset analyzed with a Gaussian covariance model).



(a) $\|\cdot\|_{\text{op}}$ -KDE point estimate.



(b) KDE-DPC decision graph.

Figures 13a and 13b show that the posterior distribution is concentrated around a single, well-defined mode corresponding to the $\|\cdot\|_{\text{op}}$ -KDE point estimate. When constructing the 90% conformal credible region, we find that it contains the empirical covariance matrix,

but, encouragingly, none of 1,000 randomly generated covariance matrices drawn from the prior.

References

Anderson, E. (1936), 'The species problem in Iris', *Annals of the Missouri Botanical Garden* **23**(3), 457–509.

Angelopoulos, A. N. & Bates, S. (2023), 'Conformal Prediction: A Gentle Introduction', *Foundations and Trends® in Machine Learning* **16**(4), 494–591.

Balocchi, C. & Wade, S. (2025), 'Understanding uncertainty in Bayesian cluster analysis', *arXiv preprint arXiv:2506.16295* .

Barrios, E., Lijoi, A., Nieto-Barajas, L. E. & Prünster, I. (2013), 'Modeling with Normalized Random Measure Mixture Models', *Statistical Science* **28**(3), 313–334.

Beraha, M., Argiento, R., Camerlenghi, F. & Guglielmi, A. (2025), 'Bayesian mixture models with repulsive and attractive atoms', *Journal of the Royal Statistical Society Series B: Statistical Methodology* p. qkaf027.

Bernardo, J. M. & Smith, A. F. M. (1994), *Bayesian Theory*, Vol. 586, Wiley Online Library.

Binder, D. A. (1978), 'Bayesian cluster analysis', *Biometrika* **65**(1), 31–38.

Bingham, E., Chen, J. P., Jankowiak, M., Obermeyer, F., Pradhan, N., Karaletsos, T., Singh, R., Szerlip, P. A., Horsfall, P. & Goodman, N. D. (2019), 'Pyro: Deep Universal Probabilistic Programming', *J. Mach. Learn. Res.* **20**, 28:1–28:6.

URL: <http://jmlr.org/papers/v20/18-403.html>

Bishop, C. M. & Bishop, H. (2024), *Deep Learning: Foundations and Concepts*, Springer Nature.

Bolfarine, H., Lopes, H. F. & Carvalho, C. M. (2025), ‘Lower-dimensional posterior density and cluster summaries for overparameterized Bayesian models’, *arXiv preprint arXiv:2506.09850* .

Buch, D., Dewaskar, M. & Dunson, D. B. (2024), ‘Bayesian level-set clustering’, *arXiv preprint arXiv:2403.04912* .

Cremaschi, A., Wertz, T. M. & De Iorio, M. (2025), ‘Repulsion, chaos, and equilibrium in mixture models’, *Journal of the Royal Statistical Society Series B: Statistical Methodology* **87**(2), 389–432.

Dahl, D. B. (2006), Model-based clustering for expression data via a Dirichlet process mixture model, in K. A. Do, P. Müller & M. Vannucci, eds, ‘Bayesian Inference for Gene Expression and Proteomic’, Cambridge University Press, pp. 201–218.

Dahl, D. B., Johnson, D. J. & Müller, P. (2022), ‘Search algorithms and loss functions for bayesian clustering’, *Journal of Computational and Graphical Statistics* **31**(4), 1189–1201.

De Blasi, P., Favaro, S., Lijoi, A., Mena, R. H., Prünster, I. & Ruggiero, M. (2013), ‘Are Gibbs-type priors the most natural generalization of the Dirichlet process?’, *IEEE transactions on pattern analysis and machine intelligence* **37**(2), 212–229.

Duan, Y., Guo, S., Yan, H., Wang, W. & Mueller, P. (2025), ‘Spatially aligned random partition models on spatially resolved transcriptomics data’, *bioRxiv* pp. 2025–04.

Dvoretzky, A., Kiefer, J. & Wolfowitz, J. (1956), ‘Asymptotic minimax character of the sample distribution function and of the classical multinomial estimator’, *The Annals of Mathematical Statistics* pp. 642–669.

Escobar, M. D. & West, M. (1995), ‘Bayesian density estimation and inference using mixtures’, *Journal of the American Statistical Association* **90**(430), 577–588.

Escobar, M. D. & West, M. (1998), Computing nonparametric hierarchical models, *in* ‘Practical nonparametric and semiparametric Bayesian statistics’, Springer, pp. 1–22.

Ester, M., Kriegel, H.-P., Sander, J., Xu, X. et al. (1996), ‘A density-based algorithm for discovering clusters in large spatial databases with noise’, *Knowledge Discovery and Data Mining* **96**(34), 226–231.

Favaro, S. & Teh, Y. W. (2013), ‘MCMC for Normalized Random Measure Mixture Models’, *Statistical Science* **28**(3), 335 – 359.

Ferraty, F. & Vieu, P. (2006), *Nonparametric Functional Data Analysis: Theory and Practice*, Springer.

Flamary, R., Courty, N., Gramfort, A., Alaya, M. Z., Boisbunon, A., Chambon, S., Chapel, L., Corenflos, A., Fatras, K., Fournier, N., Gautheron, L., Gayraud, N. T., Janati, H., Rakotomamonjy, A., Redko, I., Rolet, A., Schutz, A., Seguy, V., Sutherland, D. J., Tavenard, R., Tong, A. & Vayer, T. (2021), ‘POT: Python Optimal Transport’, *Journal of Machine Learning Research* **22**(78), 1–8.

Flamary, R., Vincent-Cuaz, C., Courty, N., Gramfort, A., Kachaiev, O., Quang Tran, H., David, L., Bonet, C., Cassereau, N., Gnassounou, T., Tanguy, E., Delon, J., Collas, A., Mazelet, S., Chapel, L., Kerdoncuff, T., Yu, X., Feickert, M., Krzakala, P., Liu, T. & Fernandes Montesuma, E. (2024), ‘POT Python Optimal Transport (version 0.9.5)’.

URL: <https://github.com/PythonOT/POT>

Fong, E. & Holmes, C. C. (2021), ‘Conformal Bayesian Computation’, *Advances in Neural Information Processing Systems* **34**, 18268–18279.

Fritsch, A. & Ickstadt, K. (2009), ‘Improved criteria for clustering based on the posterior

similarity matrix’, *Bayesian Analysis* **4**(2), 367–392.

Fruhwirth-Schnatter, S., Celeux, G. & Robert, C. P. (2019), *Handbook of mixture analysis*,

CRC press.

Gamerman, D. & Lopes, H. F. (2006), *Markov Chain Monte Carlo: Stochastic Simulation*

for Bayesian Inference, Chapman and Hall/CRC.

Grazian, C. (2023), ‘A review on bayesian model-based clustering’, *arXiv preprint*

arXiv:2303.17182 .

Hastings, W. K. (1970), ‘Monte Carlo sampling methods using Markov chains and their

applications’, *Biometrika* .

Hennig, C. (2015), ‘What are the true clusters?’, *Pattern Recognition Letters* **64**, 53–62.

Hoffman, M. D., Gelman, A. et al. (2014), ‘The no-u-turn sampler: adaptively setting path

lengths in Hamiltonian Monte Carlo’, *Journal of Machine Learning Research* **15**(1), 1593–

1623.

Jeffreys, H. (1998), *The Theory of Probability*, Oxford University Press.

Kalli, M., Griffin, J. E. & Walker, S. G. (2011), ‘Slice sampling mixture models’, *Statistics*

and Computing

21(1), 93–105.

Kappenman, E. S., Farrens, J. L., Zhang, W., Stewart, A. X. & Luck, S. J. (2021),

‘ERP CORE: An open resource for human event-related potential research’, *NeuroImage*

225, 117465.

Kass, R. E. & Raftery, A. E. (1995), ‘Bayes factors’, *Journal of the American Statistical*

Association **90**(430), 773–795.

Kriegel, H.-P., Kröger, P., Sander, J. & Zimek, A. (2011), ‘Density-based clustering’, *Wiley Interdisciplinary Reviews: Data Mining and Knowledge Discovery* **1**(3), 231–240.

Lau, J. W. & Green, P. J. (2007), ‘Bayesian model-based clustering procedures’, *Journal of Computational and Graphical Statistics* **16**(3), 526–558.

Lee, H.-O., Hong, Y., Etlioglu, H. E., Cho, Y. B., Pomella, V., Van den Bosch, B., Vanhecke, J., Verbandt, S., Hong, H., Min, J.-W. et al. (2020), ‘Lineage-dependent gene expression programs influence the immune landscape of colorectal cancer’, *Nature genetics* **52**(6), 594–603.

Lei, J., G’Sell, M., Rinaldo, A., Tibshirani, R. J. & Wasserman, L. (2018), ‘Distribution-free predictive inference for regression’, *Journal of the American Statistical Association* **113**(523), 1094–1111.

Leonard, T. & Hsu, J. S. (1992), ‘Bayesian inference for a covariance matrix’, *The Annals of Statistics* **20**(4), 1669–1696.

Levin, D. A. & Peres, Y. (2017), *Markov chains and mixing times*, Vol. 107, American Mathematical Society.

Lewandowski, D., Kurowicka, D. & Joe, H. (2009), ‘Generating random correlation matrices based on vines and extended onion method’, *Journal of Multivariate Analysis* **100**(9), 1989–2001.

Lijoi, A., Mena, R. H. & Prünster, I. (2005), ‘Hierarchical mixture modeling with normalized inverse-Gaussian priors’, *Journal of the American Statistical Association* **100**(472), 1278–1291.

Lijoi, A., Nipoti, B. & Prünster, I. (2014), ‘Bayesian inference with dependent normalized completely random measures’, *Bernoulli* **20**(3), 1260–1291.

Lijoi, A., Prünster, I. & Rigon, T. (2020), ‘The Pitman–Yor multinomial process for mixture modelling’, *Biometrika* **107**(4), 891–906.

Lo, A. Y. (1984), ‘On a class of bayesian nonparametric estimates: I. density estimates’, *The Annals of Statistics* **12**(1), 351–357.

MacEachern, S. N. (2000), ‘Dependent Dirichlet Processes’, *Unpublished manuscript, Department of Statistics, The Ohio State University* .

MacEachern, S. N. & Müller, P. (1998), ‘Estimating mixture of dirichlet process models’, *Journal of Computational and Graphical Statistics* **7**(2), 223–238.

Massart, P. (1990), ‘The tight constant in the Dvoretzky-Kiefer-Wolfowitz inequality’, *The Annals of Probability* pp. 1269–1283.

Meilă, M. (2007), ‘Comparing clusterings—an information based distance’, *Journal of Multivariate Analysis* **98**(5), 873–895.

Metropolis, N., Rosenbluth, A. W., Rosenbluth, M. N., Teller, A. H. & Teller, E. (1953), ‘Equation of state calculations by fast computing machines’, *The Journal of Chemical Physics* **21**(6), 1087–1092.

Neal, R. M. (2000), ‘Markov chain sampling methods for Dirichlet process mixture models’, *Journal of Computational and Graphical Statistics* **9**(2), 249–265.

Nguyen, K. & Mueller, P. (2024), ‘Summarizing Bayesian Nonparametric Mixture Posterior–Sliced Optimal Transport Metrics for Gaussian Mixtures’, *arXiv preprint arXiv:2411.14674* .

Nguyen, X. (2013), ‘Convergence of latent mixing measures in finite and infinite mixture models’, *The Annals of Statistics* **41**(1), 370 – 400.

Nowicki, K. & Snijders, T. A. B. (2001), ‘Estimation and prediction for stochastic block-structures’, *Journal of the American Statistical Association* **96**(455), 1077–1087.

Orbánz, P. & Roy, D. M. (2014), ‘Bayesian models of graphs, arrays and other exchangeable random structures’, *IEEE transactions on pattern analysis and machine intelligence* **37**(2), 437–461.

Page, G. L., Barrientos, A. F., Dahl, D. B. & Dunson, D. B. (2025), ‘Uncertainty quantification in bayesian clustering’, *arXiv preprint arXiv:2511.16040* .

Papaspiliopoulos, O. & Roberts, G. O. (2008), ‘Retrospective markov chain monte carlo methods for dirichlet process hierarchical models’, *Biometrika* pp. 169–186.

Perman, M., Pitman, J. & Yor, M. (1992), ‘Size-biased sampling of Poisson point processes and excursions’, *Probability Theory and Related Fields* **92**(1), 21–39.

Petralia, F., Rao, V. & Dunson, D. (2012), ‘Repulsive mixtures’, *Advances in neural information processing systems* **25**.

Phan, D., Pradhan, N. & Jankowiak, M. (2019), ‘Composable Effects for Flexible and Accelerated Probabilistic Programming in NumPyro’, *arXiv preprint arXiv:1912.11554*

Pitman, J. & Yor, M. (1997), ‘The two-parameter Poisson-Dirichlet distribution derived from a stable subordinator’, *The Annals of Probability* pp. 855–900.

Quintana, F. A. & Iglesias, P. L. (2003), ‘Bayesian clustering and product partition models’, *Journal of the Royal Statistical Society: Series B (Statistical Methodology)* **65**(2), 557–574.

Rastelli, R. & Friel, N. (2018), ‘Optimal Bayesian estimators for latent variable cluster models’, *Statistics and Computing* **28**(6), 1169–1186.

Rigon, T., Herring, A. H. & Dunson, D. B. (2023), ‘A generalized Bayes framework for

probabilistic clustering’, *Biometrika* **110**(3), 559–578.

Rodriguez, A., Dunson, D. B. & Gelfand, A. E. (2008), ‘The nested Dirichlet process’,

Journal of the American statistical Association **103**(483), 1131–1154.

Rodriguez, A. & Laio, A. (2014), ‘Clustering by fast search and find of density peaks’,

Science **344**(6191), 1492–1496.

Roeder, K. (1990), ‘Density estimation with confidence sets exemplified by superclusters

and voids in the galaxies’, *Journal of the American Statistical Association* **85**(411), 617–

624.

Sarkar, S. & Kuchibhotla, A. K. (2023), ‘Post-selection inference for conformal prediction:

Trading off coverage for precision’, *arXiv preprint arXiv:2304.06158* .

Schoenberg, I. J. (1935), ‘Remarks to Maurice Fréchet’s Article “Sur La Définition Ax-

iomatique D’Une Classe D’Espace Distancés Vectoriellement Applicable Sur L’Espace

De Hilbert’, *Annals of Mathematics* **36**(3), 724–732.

Schölkopf, B. & Smola, A. J. (2001), *Learning with Kernels: Support Vector Machines,*

Regularization, Optimization, and Beyond, MIT Press.

Selva, F., Fuentes-García, R. & Gil-Leyva, M. F. (2025), ‘pyrichlet: A Python Package

for Density Estimation and Clustering Using Gaussian Mixture Models’, *Journal of*

Statistical Software **112**, 1–39.

Shafer, G. & Vovk, V. (2008), ‘A tutorial on conformal prediction.’, *Journal of Machine*

Learning Research **9**(3).

Shawe-Taylor, J. & Cristianini, N. (2004), *Kernel Methods for Pattern Analysis*, Cambridge

University Press.

Song, Z., Camerlenghi, F., Shen, W., Guindani, M. & Beraha, M. (2025), ‘Repulsive Mixture Model with Projection Determinantal Point Process’, *arXiv preprint arXiv:2510.08838* .

Teh, Y. W., Jordan, M. I., Beal, M. J. & Blei, D. M. (2006), ‘Hierarchical Dirichlet Processes’, *Journal of the American Statistical Association* **101**(476), 1566–1581.

Tierney, L. (1994), ‘Markov chains for exploring posterior distributions’, *The Annals of Statistics* pp. 1701–1728.

Villani, C. et al. (2008), *Optimal Transport: Old and New*, Vol. 338, Springer.

Vinh, N. X., Epps, J. & Bailey, J. (2010), ‘Information theoretic measures for clusterings comparison: Variants, properties, normalization and correction for chance’, *Journal of Machine Learning Research* **11**, 2837–2854.

Vovk, V. (2012), Conditional validity of inductive conformal predictors, in ‘Asian Conference on Machine Learning’, PMLR, pp. 475–490.

Vovk, V., Gammerman, A. & Shafer, G. (2005), *Algorithmic Learning in a Random World*, Springer.

Wade, S. (2023), ‘Bayesian cluster analysis’, *Philosophical Transactions of the Royal Society A* **381**(2247), 20220149.

Wade, S. & Ghahramani, Z. (2018), ‘Bayesian Cluster Analysis: Point Estimation and Credible Balls (with Discussion)’, *Bayesian Analysis* **13**(2), 559 – 626.

Walker, S. G. (2007), ‘Sampling the Dirichlet mixture model with slices’, *Communications in Statistics—Simulation and Computation®* **36**(1), 45–54.

Wang, D., Lu, X. & Rinaldo, A. (2019), ‘DBSCAN: Optimal rates for density-based cluster estimation’, *Journal of Machine Learning Research* **20**(170), 1–50.

Woody, S., Carvalho, C. M. & Murray, J. S. (2021), ‘Model interpretation through lower-dimensional posterior summarization’, *Journal of Computational and Graphical Statistics* **30**(1), 144–161.

Xie, F. & Xu, Y. (2020), ‘Bayesian repulsive Gaussian mixture model’, *Journal of the American Statistical Association* **115**(529), 187–203.

Xu, Y., Müller, P. & Telesca, D. (2016), ‘Bayesian inference for latent biologic structure with determinantal point processes (dpp)’, *Biometrics* **72**(3), 955–964.

Yang, R. & Berger, J. O. (1994), ‘Estimation of a covariance matrix using the reference prior’, *The Annals of Statistics* pp. 1195–1211.